



The isotopic composition of atmospheric nitrous oxide observed at the high-altitude research station Jungfrauoch, Switzerland

Longfei Yu^{1*}, Eliza Harris^{1†}, Stephan Henne¹, Sarah Eggleston¹, Martin Steinbacher¹, Lukas
5 Emmenegger¹, Christoph Zellweger¹ and Joachim Mohn¹

¹Laboratory for Air Pollution & Environmental Technology, Empa, Swiss Federal Laboratories
for Materials Science and Technology, Ueberlandstr. 129, CH-8600 Duebendorf, Switzerland.

[†]Current address: Institute of Ecology, University of Innsbruck, Sternwartestrasse 15, A-6020
Innsbruck, Austria

10 * Correspondence: L. Yu (longfei.yu@empa.ch)



Abstract

Atmospheric nitrous oxide (N₂O) levels have been continuously growing since preindustrial times. Mitigation requires information about sources and sinks on the regional and global scales.

15 Isotopic composition of N₂O in the atmosphere could contribute valuable constraints. However, isotopic records of N₂O in the unpolluted atmosphere remain too scarce for large-scale N₂O models. Here, we report the results of discrete air samples collected weekly to bi-weekly over a five-year period at the high-altitude research station Jungfraujoch, located in central Switzerland. High-precision N₂O isotopic measurements were made using a recently developed

20 preconcentration-laser spectroscopy technique. The measurements of discrete samples were accompanied by *in situ* continuous measurements of N₂O mixing ratios. Our results indicate a pronounced seasonal pattern with minimum N₂O mixing ratios in late summer, associated with a maximum in $\delta^{15}\text{N}^{\text{bulk}}$ and a minimum in intramolecular ¹⁵N site preference ($\delta^{15}\text{N}^{\text{SP}}$). This pattern is most likely due to stratosphere-troposphere exchange (STE), which delivers N₂O-depleted but

25 ¹⁵N-enriched air from the stratosphere into the troposphere. Variability in $\delta^{15}\text{N}^{\text{SP}}$ induced by changes in STE may be masked by biogeochemical N₂O production processes in late summer, which are possibly dominated by a low- $\delta^{15}\text{N}^{\text{SP}}$ pathway of N₂O production (denitrification), providing an explanation for the observed seasonality of $\delta^{15}\text{N}^{\text{SP}}$. Footprint analyses and atmospheric transport simulations of N₂O for Jungfraujoch suggest that regional emissions from

30 the planetary boundary layer contribute to seasonal variations of atmospheric N₂O isotopic composition at Jungfraujoch, albeit more clearly for $\delta^{15}\text{N}^{\text{SP}}$ and $\delta^{18}\text{O}$ than for $\delta^{15}\text{N}^{\text{bulk}}$. With the time-series of five years, we obtained a significant interannual trend for $\delta^{15}\text{N}^{\text{bulk}}$ after deseasonalization ($-0.052\pm 0.012\text{‰ a}^{-1}$), indicating that the atmospheric N₂O increase is due to isotopically depleted N₂O sources. We estimated the average isotopic signature of anthropogenic



35 N₂O sources with a two-box model to be $-8.6 \pm 0.6\%$ for $\delta^{15}\text{N}^{\text{bulk}}$, $34.8 \pm 3\%$ for $\delta^{18}\text{O}$ and $10.7 \pm 4\%$
for $\delta^{15}\text{N}^{\text{SP}}$. Our study demonstrates that seasonal variation of N₂O isotopic composition in the
background atmosphere is important when determining interannual trends. More frequent, high-
precision and inter-laboratory compatible measurements of atmospheric N₂O isotopocules,
especially for $\delta^{15}\text{N}^{\text{SP}}$, are needed to better constrain anthropogenic N₂O sources, and thus the
40 contribution of biogeochemical processes to N₂O growth on the global scale.



1 Introduction

Nitrous oxide (N_2O) is a potent greenhouse gas (Fowler et al., 2015) and a strong stratospheric ozone-depleting substance (Ravishankara et al., 2009). For several decades, near-surface atmospheric N_2O mixing ratios have been continuously measured at a series of remote sites, 45 within the networks of the Global Atmosphere Watch Programme (JMA and WMO, 2018), the Advanced Global Atmospheric Gases Experiment (AGAGE) (Prinn et al., 2018), and the National Oceanic and Atmospheric Administration (NOAA) Earth System Research Laboratory (ESRL) Global Monitoring Division (GMD) (Nevison et al., 2011). These measurements have shown a significant increase in atmospheric N_2O mixing ratio, at a current growth rate of about 50 $0.93 \text{ nmol mol}^{-1} \text{ a}^{-1}$ (WMO, 2018). On the global scale, given excessive nitrogen (N) fertilizer application, agriculture is known to be the largest and most important anthropogenic source of N_2O (Reay et al., 2012; Tian et al., 2018). However, long-term observations of N_2O in the unpolluted atmosphere have shown seasonal and interannual variabilities as well as interhemispheric differences in N_2O mixing ratios (Nevison et al., 2011; Thompson et al., 2014a, 55 2014b), which cannot yet be resolved by atmospheric transport models and existing emission inventories. Moreover, regional contributions of N_2O emissions and the strengths of individual N_2O production pathways remain difficult to quantify.

Isotopic signatures of atmospheric N_2O can provide important constraints on N_2O sources (Denk et al., 2017) and trends (Kim and Craig, 1993). The ratios of $^{15}\text{N}/^{14}\text{N}$ and $^{18}\text{O}/^{16}\text{O}$ in N_2O are 60 often reported in δ notation as $\delta(^{15}\text{N}/^{14}\text{N})$ and $\delta(^{18}\text{O}/^{16}\text{O})$, abbreviated as $\delta^{15}\text{N}^{\text{bulk}}$ (average for $^{14}\text{N}^{15}\text{N}^{16}\text{O}$ and $^{15}\text{N}^{14}\text{N}^{16}\text{O}$) and $\delta^{18}\text{O}$, respectively. A large fraction of N_2O emitted to the atmosphere originates from soil bacterial processes, which usually emit N_2O that is more enriched in light (^{14}N , ^{16}O) isotopes than the tropospheric background (Pérez et al., 2001; Snider



et al., 2015a; Toyoda et al., 2017). By contrast, N₂O produced in the oceans (Bourbonnais et al.,
65 2017; Fujii et al., 2013) and emitted from fossil fuel combustion (Ogawa and Yoshida, 2005;
Toyoda et al., 2008) has higher $\delta^{15}\text{N}^{\text{bulk}}$ and $\delta^{18}\text{O}$ values which are comparable to the
tropospheric background. A recent study has summarized isotopic signatures of anthropogenic
N₂O sources divided into the EDGAR (Emissions Database for Global Atmospheric Research)
emission categories (Janssens-Maenhout et al., 2019), showing differences in isotopic signatures
70 between agricultural ($\delta^{15}\text{N}^{\text{bulk}} = -17.8$ to -1.0% and $\delta^{18}\text{O} = 23.9$ to 29%) and industrial sources
($\delta^{15}\text{N}^{\text{bulk}} = -28.7$ to 5.5% and $\delta^{18}\text{O} = 28.6$ to 40.3%) (Harris et al., 2017). These empirical
ranges, together with isotopic mixing models, provide a valuable approach to interpret variability
in atmospheric N₂O mixing ratios.

A number of studies have analyzed temporal trends in N₂O isotopic composition in the modern
75 atmosphere (Kaiser et al., 2003; Park et al., 2012; Röckmann and Levin, 2005; Toyoda et al.,
2013) and in the past from firn and ice cores (Bernard et al., 2006; Ishijima et al., 2007;
Prokopiou et al., 2018; Röckmann et al., 2003; Sowers et al., 2002). These isotopic
measurements have shown a decrease in both $\delta^{15}\text{N}^{\text{bulk}}$ - and $\delta^{18}\text{O}$ -N₂O associated with an
increasing trend in atmospheric N₂O mixing ratios since preindustrial times, indicating that the
80 recent increase of atmospheric N₂O may be due to agricultural emissions (¹⁵N and ¹⁸O depleted).
The reported trend since the 1960s seems rather steady ($-0.034 \pm 0.005 \%$ a⁻¹ for $\delta^{15}\text{N}^{\text{bulk}}$ and $-$
 0.016% a⁻¹ for $\delta^{18}\text{O}$) (Bernard et al., 2006; Ishijima et al., 2007; Park et al., 2012;
Prokopiou et al., 2017; Röckmann et al., 2003; Röckmann and Levin, 2005). However, a more
recent (1999-2010) study reported a smaller decreasing trend in $\delta^{15}\text{N}^{\text{bulk}}$ and only an insignificant
85 trend in $\delta^{18}\text{O}$ for the Northern Hemisphere (Toyoda et al., 2013). Several hypotheses were
proposed to explain the differences in the observed trends: 1) the interhemispheric difference in



N₂O emission sources results in inconsistent isotopic signatures among different studies (Thompson et al., 2014b); 2) uncertainties in isotopic measurements and variable sampling schemes (air type, sampling frequency and time) mask the small secular trend of N₂O isotopic composition in the background atmosphere (Toyoda et al., 2013); and/or 3) N₂O source isotopic signatures have changed in recent years, possibly due to shifts in N fertilizer type and climatic forcing (Tian et al., 2018). Hence, further investigation into the global N₂O source inventory and its evolution over time requires more frequent, precise measurements of N₂O isotopocules in the unpolluted atmosphere, particularly in the Northern Hemisphere.

95 Recently, site-specific composition of N₂O isotopomers (site preference: $\delta^{15}\text{N}^{\text{SP}}$), which denotes the difference of ¹⁵N between the central (¹⁴N¹⁵N¹⁶O, α position) and terminal (¹⁵N¹⁴N¹⁶O, β position) N atoms, has been applied to constrain sources contributing to atmospheric N₂O (Toyoda et al., 2013; Yoshida and Toyoda, 2000). $\delta^{15}\text{N}^{\text{SP}}$ of N₂O is particularly effective for distinguishing between the major N₂O production processes, i.e. nitrification and denitrification, generally referred to as aerobic and anaerobic N₂O production, with high and low $\delta^{15}\text{N}^{\text{SP}}$, respectively (Sutka et al., 2006). However, despite the advantages of $\delta^{15}\text{N}^{\text{SP}}$ measurements, existing long-term studies have not yet been able to reach a definitive understanding of the $\delta^{15}\text{N}^{\text{SP}}$ -N₂O trend, showing both positive (Bernard et al., 2006; Park et al., 2012; Röckmann and Levin, 2005) and negative tendencies (Röckmann et al., 2003) over the last four decades. This is probably due to an insufficient analytical precision and poor inter-laboratory agreement, in particular as the aforementioned studies are all based on isotope ratio mass spectrometry (IRMS). To retrieve site-specific isotopic information by IRMS, the N₂O⁺ molecular ions and the NO⁺ fragment ions are analyzed and raw data have to be corrected for rearrangements of central and terminal N and ¹⁷O content (Toyoda et al., 2001). Inappropriate correction algorithms and the

100
105



110 limited availability of reference materials (Ostrom et al., 2018) further enlarge the analytical
uncertainty (Mohn et al., 2014).

Seasonal variability in atmospheric N₂O isotopic composition, which could affect the longer-
term trends, is still rarely reported in the literature (Park et al., 2012; Toyoda et al., 2013).
Moreover, studies of seasonality of N₂O isotopic composition are limited to the recent past since
115 the air samples derived from firn and ice cores suffer from coarse temporal resolution (< 2
samples per year). Park et al. (2012) studied seasonality of atmospheric N₂O isotopic
composition by analyzing a set of archived air samples collected from Cape Grim (Australia)
using a sophisticated mathematical modeling approach. They found consistent seasonal patterns
in $\delta^{15}\text{N}^{\text{bulk}}$, $\delta^{18}\text{O}$ and $\delta^{15}\text{N}^{\text{SP}}$ of atmospheric N₂O, showing highest $^{15}\text{N}/^{18}\text{O}$ enrichment in June
120 and lowest in December. This pattern was negatively correlated with the seasonality of the N₂O
mixing ratios (lowest in April-May and highest in December), which is in agreement with a
previous study by Nevison et al. (2011). The negative correlation between isotopic composition
and mixing ratios has been explained by stratosphere-troposphere exchange (STE), which
transports N₂O-depleted but isotopically enriched stratospheric air (prevailing reduction process)
125 into the lower atmosphere (Yung and Miller, 1997). However, in a more recent study from
Hateruma Island (Japan), Toyoda et al. (2013) reported insignificant seasonal patterns in
atmospheric N₂O isotopocules (smaller variability than measurement precision), despite their
finding of a somewhat similar seasonal pattern in N₂O mixing ratio (minimum in July). Although
there are interhemispheric differences in N₂O sources and distinct sampling frequencies in the
130 two studies discussed above (2-3 times per year versus monthly), it is noteworthy that both
studies observed significantly larger variability in $\delta^{15}\text{N}^{\text{SP}}$ than in $\delta^{15}\text{N}^{\text{bulk}}$ and $\delta^{18}\text{O}$. Whether the
fluctuations in $\delta^{15}\text{N}^{\text{SP}}$ are mainly caused by the limited repeatability of the chosen analytical



techniques or interplay of processes or mechanisms regulating atmospheric N₂O remains to be tested (Park et al., 2012).

135 With inherent selectiveness, in particular for site-specific isotopic composition, laser spectroscopy provides a new analytical approach for direct, precise measurements of all four N₂O isotopocules (Harris et al., 2014; Mohn et al., 2012). The recent development of quantum cascade laser absorption spectroscopy (QCLAS) coupled with an automated preconcentration unit has been applied to measure N₂O isotopocules in ambient air, with comparable precision for

140 $\delta^{15}\text{N}^{\text{bulk}}$ and $\delta^{18}\text{O}$ and superior precision for $\delta^{15}\text{N}^{\text{SP}}$ relative to IRMS systems (Harris et al., 2017; Mohn et al., 2014). Here, we present results from the application of a preconcentration unit coupled to QCLAS to measure atmospheric N₂O isotopocules in background air collected at the high altitude research station Jungfraujoch, Switzerland. Between April 2014 and December 2018, we collected weekly to bi-weekly air samples for N₂O isotopic analyses, in parallel with

145 online measurement of N₂O mixing ratios. To our knowledge, this work reports the first time-series of background atmospheric N₂O isotopic composition using laser spectroscopy. With this unique dataset, we aim to 1) constrain seasonal patterns of three N₂O isotopic signatures at the Jungfraujoch observatory; 2) determine interannual trends in N₂O isotopocules, especially $\delta^{15}\text{N}^{\text{SP}}$; and 3) interpret the observed patterns in N₂O mixing ratios using temporal trends in N₂O isotopic

150 composition and reported isotopic signatures of anthropogenic sources.



2 Materials and Method

2.1 Site description

The high altitude research station Jungfraujoch (3580 m above sea level), located on the northern ridge of the Swiss Alps, is a well-established site for studying unpolluted atmosphere over
155 Central Europe (e.g. Buchmann et al., 2016). Although the station is located in the free troposphere most of the time, it is occasionally affected by air recently lifted from the planetary boundary layer (Herrmann et al., 2015; Zellweger et al., 2003). Henne et al. (2010) investigated the representativeness of 35 European monitoring stations and categorized Jungfraujoch as “mostly remote”. The Jungfraujoch station is part of several national and international networks,
160 like the meteorological SwissMetNet network operated by MeteoSwiss, the Swiss National Air Pollution Monitoring Network (NABEL), the Global Atmospheric Watch Programme (GAW) of the World Meteorological Organization (WMO) and the Integrated Carbon Observation Systems (ICOS) Research Infrastructure. This results in an extended set of long-term and continuously available parameters such as meteorological variables (Appenzeller et al., 2008), greenhouse
165 gases (Schibig et al., 2015; Sepúlveda et al., 2014; Yuan et al., 2018), CO₂ isotopic composition (Sturm et al., 2013; Tuzson et al., 2011), ozone-depleting substances and their replacement products (Reimann et al., 2008), atmospheric pollutants (Logan et al., 2012; Pandey Deolal et al., 2012; Zellweger et al., 2009) and aerosol parameters (Bukowiecki et al., 2016).

2.2 *In situ* measurements and discrete air sampling (flasks)

170 *In situ* observations of N₂O mixing ratios commenced at Jungfraujoch in December 2004. Initially, measurements were made with gas chromatography (GC) (Agilent 6890N, USA) followed by electron capture detection (ECD). The time resolution of these measurements was



24 to 30 minutes. In late 2014, we implemented a cavity-enhanced off-axis integrated cavity out-
put spectroscopy analyzer (OA-ICOS, Los Gatos Research Inc., Mountain View, CA, USA),
175 which measures the atmospheric N₂O mixing ratio continuously. Due to the superior
measurement precision compared to the GC-ECD method (Lebague et al., 2016), the OA-ICOS
record has become the primary time-series since January 2015. The GC-ECD observations
continued until summer 2016 for comparison and quality control.

Additional parameters, recorded within the NABEL network and the ICOS infrastructure, were
180 included in the analysis below. These data were carbon monoxide (CO) (measured by cavity
ring-down spectroscopy; Model G2401, Picarro Inc., USA), the sum of oxidized nitrogen species
(NO_y) (measured by chemiluminescence detection after conversion of NO_y to NO on a heated
gold catalyst; CLD 89p, Eco Physics, Switzerland) and O₃ (measured by UV absorption; TEI 49i,
Thermo Scientific, USA).

185 In conjunction with the online measurements, we deployed an automated sampling system (Fig.
S1) to collect pressurized air samples in aluminum cylinders from the same air inlet at the Sphinx
observatory, for subsequent N₂O mixing ratio and isotopic analyses. The sample collection was
conducted weekly from April 2014 to February 2016. After a sampling gap of five months due to
a technical failure, we reinitiated a bi-weekly sampling, which continued from August 2016 to
190 December 2018. The sampling system, automated by a customized LabVIEW program (National
Instruments Corp., USA), consisted of a Nafion drier (PD-100T-48MSS, Perma Pure LLC, USA),
a membrane gas compressor (KNF Neuberger, USA; Type N286 series), a 16-port selector valve
(EMT2CSD16MWEPP, VICI AG, Switzerland), and a rack to accommodate nine 2-L aluminum
flasks (Luxfer, Messer Schweiz AG, Switzerland). During sample filling, pre-evacuated flasks
195 were first purged with ambient air five times (1 hour), and then filled to 12000 hPa within 40



min, resulting in approximately 24 L (298 K and 1000 hPa) of air per flask for isotopic analysis. Air sample filling generally took place between 2:00 and 3:00 pm local time at each sampling day. Sample flasks were sent back to the laboratory at Empa for analyses every few months. For this study, 142 air samples were collected in flasks and analyzed for N₂O isotopocules.

200 2.3 Analyses of discrete air samples

Discrete air samples were regularly analyzed in batches but note in chronological order to prevent the imprint of analytical drifts on temporal trends of the samples. N₂O mole fractions were analyzed by QCLAS (CW-QC-TILDAS-76-CS, Aerodyne Research Inc., USA) against NOAA standards on the WMO-X2006A calibration scale (Hall et al., 2007), at a precision
205 around 0.1 nmol mol⁻¹ (determined with the average of 1-min data).

The four most abundant N₂O isotopocules (¹⁴N¹⁴N¹⁶O, 99.03%; ¹⁴N¹⁵N¹⁶O, 0.36%; ¹⁵N¹⁴N¹⁶O, 0.36%; ¹⁴N¹⁴N¹⁸O, 0.20%) were analyzed using a customized QCLAS system (Aerodyne Research, Inc., USA) (Heil et al., 2014) coupled with an automated preconcentration device (Mohn et al., 2010). Before entering the pre-concentration unit, sample air is passed through a
210 Sofnocat 423 trap (Molecular Products Limited, GB) to remove CO, and subsequently through an Ascarite trap (Ascarite: 6 g, 10–35 mesh, Sigma Aldrich, Switzerland, bracketed by Mg(ClO₄)₂, 2 × 1.5 g, Alfa Aesar, Germany) to remove CO₂ and water. Approximately 5.5 L of air with a flow of 250 ml min⁻¹ (at 295 K and 3500 hPa) is then passed through a HayeSep D trap cooled to -145 °C to collect N₂O (Mohn et al., 2010). For N₂O release to the multipath cell of the
215 QCLAS, the HayeSep D trap is quickly heated to 10 °C and flushed with high-purity synthetic air (20.5% of O₂ in N₂) carrier gas at a flow rate of 25 ml min⁻¹ (at 295 K and 3500 hPa). A final cell pressure around 16 hPa is achieved, which results in an N₂O mixing ratio of about 45 μmol mol⁻¹. More instrumental details can be found in previous studies (Harris et al., 2017; Mohn et al., 2010,



2012). Sample tanks were each analyzed twice to yield duplicates for N₂O isotopic results, which
220 left sufficient air for amount fraction analysis as described in the previous paragraph.

2.4 Data analyses

We used 10-minute averages of the continuous *in situ* measurements from the Jungfraujoch
station across this study. For a point-to-point comparison of continuous and discrete
measurements of N₂O mixing ratio, we aggregated 10-minute averages of *in situ* data for the
225 same period when the discrete sample was filled into the cylinder (40 min).

In this study, we report abundances of N₂O isotopocules using δ notation (‰) as below:

$$\delta X = \frac{(R_{sample} - R_{standard})}{R_{standard}} \quad (1)$$

where X refers to ¹⁵N^α (¹⁴N¹⁵N¹⁶O), ¹⁵N^β (¹⁵N¹⁴N¹⁶O) and ¹⁸O (¹⁴N¹⁴N¹⁸O); R refers to the ratio
between the amount fractions of the rare isotopocules as mentioned above and the amount
230 fraction of ¹⁴N¹⁴N¹⁶O; isotope standards refer to atmospheric N₂ for ¹⁵N and Vienna Standard
Mean Ocean Water (VSMOW) for ¹⁸O.

Hence, the total ¹⁵N content of N₂O and site-specific composition of N₂O isotopomers could be
further illustrated as $\delta^{15}\text{N}^{bulk}$ and $\delta^{15}\text{N}^{SP}$, respectively, according to the equations below:

$$\delta^{15}\text{N}^{bulk} = (\delta^{15}\text{N}^{\alpha} + \delta^{15}\text{N}^{\beta})/2 \quad (2)$$

$$235 \quad \delta^{15}\text{N}^{SP} = \delta^{15}\text{N}^{\alpha} - \delta^{15}\text{N}^{\beta} \quad (3)$$

Two standards (CG1, CG2) with distinct isotopic signatures ($\delta^{15}\text{N}^{\alpha} = 16.29 \pm 0.07\text{‰}$ (CG1) and
-51.09 ± 0.07‰ (CG2); $\delta^{15}\text{N}^{\beta} = -2.59 \pm 0.06\text{‰}$ and -48.12 ± 0.04‰; $\delta^{18}\text{O} = 39.37 \pm 0.04\text{‰}$ and
30.81 ± 0.03‰) were used for calibrating isotopic composition. The calibration gases CG1 and



CG2 were calibrated on the Tokyo Institute of Technology (TIT) scale, based on cross-
240 calibration with primary standards assigned by TIT (Mohn et al., 2012, 2014). In addition, CG1
was measured repeatedly between samples and target gases to account for instrumental drift.
Both CG1 and CG2 have N₂O mixing ratios of 45 μmol mol⁻¹, similar to the N₂O amount
fraction of the samples after preconcentration. However, to correct for possible instrumental
dependence on N₂O mixing ratio, CG1 was diluted to N₂O mole fractions of 35-40 μmol mol⁻¹
245 within each measurement batch. In general, duplicated isotopic measurements of flask samples
yielded values of repeatability of 0.10-0.20‰ for δ¹⁵N^{bulk} and δ¹⁸O, and 0.15-0.25‰ for δ¹⁵N^{SP}.

At the beginning of the project, a batch of three cylinders (50 L water volume, Luxfer, Italy)
were filled with pressurized ambient air in Dübendorf with an oil-free, three stage compressor
(SA-3, Rix Industries, USA) and used as long-term target gases. The pressurized ambient air
250 target gas was analyzed with identical treatment as Jungfraujoch air samples during every
analysis batch, to monitor long-term analytical drift. Standard deviations for repeated target gas
measurements throughout the period of Jungfraujoch sample measurements, were 0.13‰ for
δ¹⁵N^{bulk}, 0.21‰ for δ¹⁵N^{SP}, and 0.11‰ for δ¹⁸O (Fig. S2).

2.5 Surface air footprint analysis and simulated regional N₂O enhancement

255 We analyzed the air mass origin at Jungfraujoch by applying the Lagrangian particle dispersion
model (LPDM) FLEX-PART in the backward mode (Stohl et al., 2005). The model was driven
by meteorological fields taken from the ECMWF-IFS operational analysis cycle, extracted at a
resolution of 1°×1°, 90/137 levels globally, and at higher horizontal resolution of 0.2°×0.2° for
central Europe. We released 50000 virtual air parcels every 3 hours at 3000 m a.s.l. from
260 Jungfraujoch to perform backward dispersion simulations over 10 days, which allowed us to



calculate surface source sensitivities (concentration footprints). A release height of 3000 m a.s.l. was previously determined to be an optimum for simulating concentration footprints at Jungfraujoch, given the stated horizontal resolution which results in a considerable smoothing of the complex, alpine orography (Keller et al., 2012). The 3-hourly surface footprints for the whole
265 observation period were used to categorize different transport regimes using the clustering approach outlined in Sturm et al. (2013). This allowed us to distinguish among six different source regions: Free Troposphere (FT), Southwest (SW), East (E), Local (L), West (W) and Northwest (NW).

Similar to Henne et al. (2016) for CH₄ and based on spatially resolved N₂O emission inventories
270 (Meteotest for Switzerland; EDGAR for Europe), we used the FLEXPART concentration footprints to calculate time-series of atmospheric mole fraction increases at Jungfraujoch resolved by emission sectors (Henne et al., 2016). The emission inventory by Meteotest consists of 12 emission sectors, among which all sectors except “organic soils” are comparable to sectors in the EDGAR inventory (See Table S2) (Janssens-Maenhout et al., 2019). To improve seasonal
275 representation of the emissions in our model, we used a monthly resolved, optimized version of the emission inventory, which was obtained through inverse modeling using the N₂O atmospheric mole fractions observed between March 2017 and September 2018 at the tall tower site Beromuenster on the Swiss plateau (Henne et al., 2019). Therefore, in this study, source contributions to Jungfraujoch were estimated specifically for the period mentioned above.

280 **2.6 Evaluation of seasonal pattern and interannual trend for time-series**

To explore seasonality and interannual trends, we fit the time-series of *in situ* measurements of N₂O and O₃ mixing ratios, NO_y-to-CO ratios and isotopic measurements of N₂O with polynomial



functions and Fourier series (four harmonics for *in situ* measurements and two harmonics for discrete measurements) (Thoning et al., 1989). Time-series were then decomposed into a linear
285 trend, seasonal variability (per 12 months) and residuals. This fit was conducted with a nonlinear least-squares (NLS) model with R-3.5.3 (R Core Team, 2016). The detrended seasonality was examined by comparing peak-to-peak amplitudes with our analytical precisions and the uncertainty given by the one standard deviation of monthly residuals. To determine interannual trends, a linear regression was applied to both the raw and the deseasonalized datasets. The
290 significance level is set to $p < 0.01$. The interannual trends for N_2O mixing ratios were found to be little affected by seasonality, so growth rates were determined only based on the raw datasets.

Although Jungfraujoch is a remote site, episodic influence from the planetary boundary layer can be observed at the station (Pandey Deolal et al., 2012; Zellweger et al., 2003). For evaluating trends of N_2O mixing ratio measurements, we filtered out *in situ* data with significant influence
295 of planetary boundary layer, in order to represent a major air mass footprint from the free troposphere (FT). In addition to the air transport regimes, an alternative filtering criteria for the free troposphere was based on the published mean ranges of NO_y mixing ratios (501-748 ppt depending on the season) and NO_y to CO ratios (0.003-0.005 depending on the season) at Jungfraujoch (Zellweger et al., 2003). This criterion is less strict than that given by footprint
300 analyses (Herrmann et al., 2015). After applying this criterion to the isotopic time-series (which led to the exclusion of 32 measurement points), we re-evaluated the seasonal and interannual trends in the N_2O isotopic composition. In addition, because of the strong variability observed for isotopic data during the first 1.5 years (until February 2016), we performed an independent evaluation for the time-series starting from August 2016.

305 2.7 Two-box model simulation



A two-box model representing a well-mixed troposphere and stratosphere was used to estimate the anthropogenic N₂O source strength and isotopic composition from the trends measured at Jungfraujoch, similar to the approaches used by several previous studies (Ishijima et al., 2007; Röckmann et al., 2003; Schilt et al., 2014; Sowers et al., 2002). The input variables used to run
310 the model are given in Table S1. 200 iterations of the model were run using a Monte Carlo-style approach to approximate the uncertainty considering the uncertainty distribution for each input variable as given in Table S1. All variables were set independently within the Monte Carlo approximation except for preindustrial N₂O life time (T_{PI}), which was fixed to 106% of the present-day N₂O life time T_{PD} (Prather et al., 2015).

315 Within each iteration of the model, the preindustrial N₂O burden was first described, assuming steady state in the preindustrial era. The preindustrial stratospheric N₂O mixing ratio ($c_{S,PI}$) ($270 \pm 7.5 \text{ nmol mol}^{-1}$) was taken from Sowers et al. (2002):

$$0 = TS_{\text{ex}} (c_{PI} - c_{S,PI}) - (M_{PI} + M_{S,PI})/\tau_{PI} \quad (4)$$

where TS_{ex} refers to the troposphere-stratosphere exchange rate; c_{PI} refers to the preindustrial
320 tropospheric N₂O mixing ratio; and M_{PI} and $M_{S,PI}$ are the masses of N₂O in the troposphere and stratosphere respectively. The preindustrial terrestrial flux in Sowers et al. (2002) (equation 2) was used here assuming no anthropogenic emissions. The delta values for the preindustrial stratosphere and the fractionation factor for the stratospheric sink were taken from equations 6 and 7 from Sowers et al. (2002) assuming steady state and no anthropogenic emissions. The
325 model was run with a yearly time step starting from the preindustrial assuming that anthropogenic emissions began in 1845 (Sowers et al., 2002). For each year of the model run, the



anthropogenic flux was calculated according to the exponential increase described by Sowers et al. (2002):

$$F_{\text{anth},t} = e^{\alpha(t-t_0)} - 1 \quad (5)$$

330 where t is the current year, $t_0 = 1845$ and α is the growth rate (assumed to be constant). The rates of change for tropospheric and stratospheric N_2O mixing ratios were then retrieved from equations 2 and 3 in Sowers et al. (2002), and for the isotopic composition of stratospheric and tropospheric N_2O from equations 6 and 7 in Sowers et al. (2002).

The values of the parameters describing the anthropogenic flux were optimized to fit both the
335 trend and the absolute values for the five years of Jungfraujoch isotope data, and the mixing ratio data from the Jungfraujoch flasks and *in situ* data since 2005 (GAW data source). The uncertainties in α and in the anthropogenic source isotopic signatures were approximated by one standard deviation of values derived from repeated model runs.

2.8 “Bottom-up” estimates of source isotopic signatures

340 To gauge the accuracy of the two-box model, we deployed a “bottom-up” approach as an alternative method of estimating the N_2O source signatures. The isotopic signatures of most N_2O source sectors given in the Meteoest/EDGAR emission inventory are available from the literature, except for the “Refinery” (Table S2). As “Refinery” generally contributes only about 0.02% of the N_2O emission at Jungfraujoch, it was excluded for source isotopic signature
345 estimation. The simulated N_2O emissions by variable sources were categorized according to the EDGAR emission types (Janssens-Maenhout et al., 2019). We then calculated isotopic signatures for the overall source and the anthropogenic sources alone (excluding indirect natural emission) as weighted averages.



3 Results

350 3.1 Atmospheric N₂O mixing ratios at Jungfraujoch

We observed a linear growth of atmospheric N₂O at Jungfraujoch during the period 2014-2018 (Fig. 1a). A point-to-point comparison of discrete and *in situ* measurements showed good agreement, in particular for the second half of the study (2016-2018), where the data quality of *in situ* measurements was largely improved due to the implementation of the more precise laser spectroscopy method as compared to GC-ECD (Fig. S3). The improvement in analytical precision for N₂O mixing ratio was due to better temporal coverage by the OA-ICOS instrument, in contrast with the GC analyses which conduct one measurement per 24-30 minutes. The annual growth rates from 2014 to 2018 determined with *in situ* measurements were 0.880 ± 0.001 and 0.993 ± 0.001 nmol mol⁻¹ a⁻¹ with and without GC-ECD measurements in 2014, respectively.

360 These rates are in agreement with the global mean growth rate for the recent decade reported by NOAA (0.93 nmol mol⁻¹ a⁻¹). If we filter the *in situ* dataset to examine only the “free troposphere” periods, we obtain a lower increase (0.858 ± 0.002 nmol mol⁻¹ a⁻¹). By comparison, the annual growth rate determined from the discrete gas samples was even lower (0.813 ± 0.027 nmol mol⁻¹ a⁻¹).

365 A significant seasonal pattern was observed for N₂O mixing ratios measured *in situ*, with a maximum in early summer and a minimum in late summer (Fig. 1b). For discrete N₂O measurements a similar trend was observed, but the detrended seasonality was not significant, which might be due to the much lower number of samples (Fig. S4).

3.2 Interannual trends of N₂O isotopic composition and anthropogenic source signatures



370 Time-series of $\delta^{15}\text{N}^{\text{bulk}}$, $\delta^{15}\text{N}^{\text{SP}}$ and $\delta^{18}\text{O}$ for atmospheric N_2O at Jungfraujoch are shown in Figure 2. The NLS model simulation accounts well for the variabilities of isotopic time-series. Interannual trends of three isotopic deltas were determined for both raw and deseasonalized datasets by linear regression (Table 1). The deseasonalized interannual trends were slightly smaller than the trends determined with the raw datasets. For the whole dataset, the

375 deseasonalized trend indicates a significant decrease in $\delta^{15}\text{N}^{\text{bulk}}$, of $-0.052 \pm 0.012\% \text{ a}^{-1}$. In contrast, deseasonalized time-series of $\delta^{15}\text{N}^{\text{SP}}$ and $\delta^{18}\text{O}$ increased, albeit insignificantly, by $0.065 \pm 0.027\% \text{ a}^{-1}$ and $0.019 \pm 0.011\% \text{ a}^{-1}$, respectively. The trends determined for periods with major air mass footprints from the free troposphere were close to those calculated for the whole dataset, except that $\delta^{15}\text{N}^{\text{SP}}$ trends decreased after filtering out the samples with significant impact from plenary

380 boundary layer. This indicates that N_2O interannual trends observed at Jungfraujoch are of regional relevance, despite the fact that a small impact from local sources can be seen. Because of the observed irregular variability and the change in sampling frequency (though no change in daily sampling time) in our dataset, we separated the time-series into two phases: April 2014–February 2016 (first phase; weekly sampling) and August 2016–December 2018 (second phase;

385 bi-weekly sampling). In the first phase, the rates of increase in $\delta^{15}\text{N}^{\text{SP}}$ and $\delta^{18}\text{O}$ were almost one order of magnitude larger than over the whole dataset. This is most likely due to the unexpectedly low $\delta^{15}\text{N}^{\text{SP}}$ and $\delta^{18}\text{O}$ in summer 2014 followed by a distinct increase in winter 2014–2015, which results in large rates of increase over short periods. Such growth rates were not seen in the second phase, when both $\delta^{15}\text{N}^{\text{SP}}$ and $\delta^{18}\text{O}$ showed small and insignificant

390 variations. $\delta^{15}\text{N}^{\text{bulk}}$ displayed a decreasing interannual trend in both phases; however, the rate of decrease was larger in the second phase ($-0.130 \pm 0.045\% \text{ a}^{-1}$).



We tuned our two-box model to best match the observed N₂O mixing ratios and isotopic composition at Jungfraujoch. An estimate of anthropogenic emissions and source signatures is given in Table 2. For 2018, annual N₂O emissions were estimated to be 8.6±0.6 Tg N₂O-N a⁻¹.

395 The average isotopic signatures for anthropogenic sources were -8.6±4‰, 34.8±3‰ and 10.7±4‰ for δ¹⁵N^{bulk}, δ¹⁵N^{SP} and δ¹⁸O, respectively, which are clearly lower than those for preindustrial N₂O in the tropospheric background (Table S1; Toyoda et al., 2013).

3.3 Seasonal variation of N₂O isotopic composition

δ¹⁵N^{SP} of N₂O showed the most pronounced variability among all isotopic time-series (Fig. 2),
400 spanning 2.5‰ for individual flask sample measurements. Seasonal variability was estimated with the NLS model and presented as mean seasonal cycles (Fig. 3). For δ¹⁵N^{SP} a “summer minimum” was found regardless of whether the entire dataset or only the second phase was considered (Fig. 3), although seasonal variability of the second time-series was smaller and showed the minimum occurring earlier. The seasonal pattern of δ¹⁵N^{bulk} determined from the
405 whole dataset indicates a significant summer maximum, but this was not seen when only the data from the second phase was taken, as there was no significant seasonal pattern over this period alone. For δ¹⁸O, we observed only small temporal variability and a lack of seasonal pattern. In addition, seasonal variations of time-series filtered for free troposphere were evaluated; these show temporal patterns similar to the whole dataset (Fig. S5).

410 3.4 Air mass origin and *in situ* measurements at Jungfraujoch

Back-trajectory simulations indicate six major transport clusters during 2014-2018, as shown in Figure 4a. Four of these transport regimes (SW, E, L and NW) dominate, accounting for about 60-90% coverage of the whole period. By contrast, the free troposphere cluster only represents



10-20% of the data. Averaged monthly contributions of transport clusters are shown in Figure 4b,
415 with more pronounced impact by the L, E and NW regions in summer and stronger contribution
by FT and SW in winter. The source patterns of the air masses at Jungfraujoch were generally
consistent across the years in the present study. However, an apparent discrepancy was found for
discrete sampling times in the last two years (e.g. particularly low contribution from SW) which
is most likely due to the low and variable sampling frequency of the discrete sample collection
420 (Fig. 4b).

The detrended seasonal variability of *in situ* measurements indicates summer maxima for O₃ and
NO_y mixing ratios as well as NO_y-to-CO ratios at Jungfraujoch (Fig. S6). This likely indicates
stronger exchange with the polluted planetary boundary layer in summer (Tarasova et al., 2009),
which is consistent with the seasonal pattern of air mass footprint derived from back-trajectory
425 simulations. On the other hand, CO shows a maximum in early spring and decreases in summer
when its atmospheric lifetime is shortest. Atmospheric O₃, NO_y and CO measurements during
our discrete sampling periods also well represented seasonal variability shown for *in situ*
measurements, except for 2016-2017 where there was a five-month sampling gap (Fig. S6).

Comparisons of air mass footprints as well as O₃, NO_y and CO mixing ratios between *in situ* and
430 discrete sampling indicate that the discrete sampling covers the main air source regions and
variabilities in local pollution/free troposphere fairly well (Fig. 4 and S6). In the second phase
(2016-2018), the less frequent sampling impedes evaluation of the seasonal and interannual
variabilities.

3.5 Relationship between N₂O isotopic signatures and air mass footprints



435 We categorized N₂O mixing ratio and isotopic signature time-series into subsets based on the six
air mass transport clusters. One-way ANOVA among clusters indicates that N₂O mixing ratios in
air masses originating from cluster L were significantly higher and those from clusters FT and W
were significantly lower than the others (Fig. S7). In accordance with the pattern found for
mixing ratios, $\delta^{15}\text{N}^{\text{SP}}$ and $\delta^{18}\text{O}$ were high for cluster FT, and low for cluster L. For $\delta^{15}\text{N}^{\text{bulk}}$, little
440 difference between transport clusters was detected.



4 Discussion

4.1 Quality assurance of isotopic measurements

This study reports the first results of background N₂O isotopic measurements based on a laser spectroscopic technique. Benefiting from the preconcentration process, we achieved
445 measurement repeatability for a target gas of 0.10-0.20‰ for $\delta^{15}\text{N}^{\text{bulk}}$ and $\delta^{18}\text{O}$ (Fig. S2), which is comparable to that of IRMS measurements of ambient atmosphere (Park et al., 2012; Prokopiou et al., 2017; Röckmann et al., 2003; Toyoda et al., 2013). The long-term robustness of our technique is adequate for disentangling both seasonal and interannual temporal variability as shown in Figure 2. In particular, our analytical repeatability for $\delta^{15}\text{N}^{\text{SP}}$ (0.15-0.25‰) appears to
450 be better than previous studies measuring background atmosphere or firn air (0.8‰, Park et al., 2012; 0.3‰, Prokopiou et al., 2017; 0.3‰, Toyoda et al., 2013).

4.2 Seasonal variabilities of atmospheric N₂O isotopic composition

In situ measurements of N₂O mixing ratios showed a clear early summer maximum and late summer minimum (Fig. 1). Such a seasonal pattern was previously found for a number of NOAA
455 and AGAGE sites analyzing long-term N₂O records in the NH (Jiang et al., 2007; Nevison et al., 2011). One explanation of the late-summer minimum is a strong influence of the STE process in this period, which transports N₂O-depleted but isotopically enriched air downward from the stratosphere into the troposphere (Decock and Six, 2013). During the late summer at Jungfraujoch, we find strong enrichment of ¹⁵N in atmospheric N₂O according to the detrended
460 seasonality for the whole dataset (Fig. 3). At Hateruma Island, Japan, Toyoda et al. (2013) observed a seasonal pattern of atmospheric N₂O mixing ratios almost identical to our study, but found insignificant variations of isotopic composition. On the other hand, N₂O seasonal



variability could be influenced by oceanic emission sources (Jiang et al., 2007; Nevison et al., 2005), complicating the underlying mechanisms for the observed patterns. For example, in
465 another study looking at archived air from Cape Grim, Australia, Park et al. (2012) detected an April-May minimum and a November-December maximum for N₂O. This is expected for the SH, as STE is most prevalent in April (Nevison et al., 2011). They observed negative correlations of $\delta^{15}\text{N}^{\text{bulk}}$, $\delta^{15}\text{N}^{\alpha}$ and $\delta^{18}\text{O}$ with N₂O mixing ratios, appearing to support the idea that the STE process is responsible for seasonal variabilities in N₂O mixing ratios and isotopic composition at
470 Cape Grim. However, the seasonal cycle for $\delta^{15}\text{N}^{\alpha}$ was much larger than $\delta^{15}\text{N}^{\text{bulk}}$ and $\delta^{18}\text{O}$, which could not be explained by STE alone. They suggested that the seasonal patterns of N₂O isotopes at Cape Grim may be due to mixing between oceanic sources (high N₂O with low ¹⁵N and ¹⁸O) and STE (low N₂O with high ¹⁵N and ¹⁸O) (Nevison et al., 2011; Park et al., 2012). However, because we observe a concurrent minimum of $\delta^{15}\text{N}^{\text{SP}}$ and maximum of $\delta^{15}\text{N}^{\text{bulk}}$ in
475 July-August with low N₂O at Jungfraujoch (Fig. 3), additional mechanisms must be considered here.

Regional model simulations based on Swiss N₂O emissions derived from the inverse method were used to explore contributions from different sources to the variability in N₂O enhancements at Jungfraujoch. As shown in Figure 5a&b, soil emissions, including direct and indirect
480 emissions from agricultural lands and emissions from (semi-)natural areas, account for more than 70% of the total N₂O enhancements, while manure and waste management contribute another 20%. Total N₂O enhancements appeared to be highest in May to July (Fig. 5c), in accordance with the highest contribution by soil emissions. The early-to-middle summer maximum in the simulated N₂O enhancements is comparable with maximum of N₂O mixing ratios in early
485 summer as observed at Jungfraujoch (Fig. 1b). This underlines the importance of soil emission in



accounting for atmospheric N₂O variability (Saikawa et al., 2014). Soil N₂O emissions are mainly derived from denitrification and nitrification, which prevail in anaerobic and aerobic soil environment, respectively (Butterbach-Bahl et al., 2013). Denitrification-derived N₂O is expected to be about 30‰ lower in $\delta^{15}\text{N}^{\text{SP}}$ than N₂O produced by nitrification (Sutka et al., 2006).

490 Previous field studies at Swiss grasslands have demonstrated that low- $\delta^{15}\text{N}^{\text{SP}}$ N₂O emissions, i.e. following the denitrification pathway, dominates peak N₂O fluxes observed in summer periods (Ibraim et al., 2019). Therefore, we hypothesize that the observed minimum of $\delta^{15}\text{N}^{\text{SP}}$ in late summer at Jungfrauoch is largely contributed by the prevailing N₂O production by denitrification. By contrast, the influence of biogeochemical processes (nitrification and

495 denitrification) on $\delta^{15}\text{N}^{\text{bulk}}$ is generally smaller than that on $\delta^{15}\text{N}^{\text{SP}}$ (Toyoda et al., 2011), and such effect on $\delta^{15}\text{N}^{\text{bulk}}$ are usually overwritten by the wide range of isotopic signatures in soil N substrates (Sutka et al., 2006). Hence, given the distinct $\delta^{15}\text{N}^{\text{bulk}}$ maximum and N₂O minimum in late summer during our observation (Figs. 1 and 3), we suggest that the STE process is mainly responsible for the seasonal variability in $\delta^{15}\text{N}^{\text{bulk}}$.

500 The footprint analyses based on air mass residence time revealed a seasonal pattern, with a higher contribution of background air from the FT and SW regions in winter and more pronounced contribution of local planetary boundary layer air from the L, E and NW regions in summer (Fig. 4b). The higher frequency of air mass footprints recently in contact with the surface in summer is consistent with inverse modeling results, indicating a larger contribution of

505 soil N₂O emissions in June/July (Fig. 5). For the air mass regime representing the free troposphere, N₂O mixing ratios observed at Jungfrauoch were significantly below the average, while $\delta^{15}\text{N}^{\text{SP}}$ and $\delta^{18}\text{O}$ were higher (Fig. S7). By contrast, the local cluster (L) representing a strong impact from the planetary boundary layer had higher N₂O mixing ratios and lower



isotopic signatures (except $\delta^{15}\text{N}^{\text{bulk}}$) than the other source regions. In addition, the ratios of NO_y
510 to CO , which is a more straight-forward indicator of the free troposphere (Zellweger et al., 2003),
show significant negative correlations with $\delta^{15}\text{N}^{\text{SP}}$ and $\delta^{18}\text{O}$, but not with $\delta^{15}\text{N}^{\text{bulk}}$ (Fig. S8). This
further suggests that the seasonal variability of $\delta^{15}\text{N}^{\text{SP}}$ and $\delta^{18}\text{O}$ observed at Jungfraujoch is most
likely influenced by ground-derived emissions, while fluctuations in N_2O mixing ratios and
 $\delta^{15}\text{N}^{\text{bulk}}$ are possibly driven by STE. Considering the complexity in mechanisms responsible for
515 N_2O isotopic variations, we strongly recommend more field measurements of N_2O isotopic
signatures, in order to cover spatial and temporal variability in N_2O sources. Also, the
uncertainty in seasonal patterns could be further reduced by longer and more frequent isotopic
measurements – *in situ* monitoring at background sites like Jungfraujoch could be especially
useful.

520 Based on our bottom-up approach, we simulated isotopic signatures for the overall N_2O sources
responsible for the N_2O mixing ratio increase in the atmosphere (Fig. S9). However, the
interpretation of simulated versus observed variability in N_2O isotopic composition was difficult,
except for the somewhat similar patterns in $\delta^{18}\text{O}$. Our results suggest a limitation in the current
knowledge and literature values on isotopic signatures of most N_2O sources. In addition, most
525 N_2O sources may not exhibit a well-defined isotopic signature but a range of values regulated
under a number of processes/environmental factors. For example, isotopic signatures of soil-
derived N_2O are often determined by an interaction of several soil and climatic factors. It might
be possible in the future to model these changes implementing isotopes in ecosystem models, as
recently demonstrated by Denk et al. (2019).

530 **4.3 Interannual trends of atmospheric N_2O isotopic composition**

Over a period of almost five years, our observations show an interannual increase in N_2O mixing



ratio and decrease in $\delta^{15}\text{N}^{\text{bulk}}$ (Fig. 6). This is to be expected, assuming that the atmospheric N_2O increase is primarily attributed to anthropogenic sources, which emit isotopically lighter N_2O relative to the tropospheric background (Table S2) (Rahn and Wahlen, 2000). Compared to
535 several studies on firn air (Ishijima et al., 2007; Röckmann et al., 2003) and surface air (Park et al., 2012; Röckmann and Levin, 2005; Toyoda et al., 2013), the rate of decrease for $\delta^{15}\text{N}^{\text{bulk}}$ at Jungfraujoch is relatively high (-0.05 to 0.06 ‰ a⁻¹, Table 1). Such a discrepancy in the $\delta^{15}\text{N}^{\text{bulk}}$ trend could be due to a large contribution of terrestrial N_2O emission from the European continent to Jungfraujoch (Figs. 1 and 5), as N_2O originating from soil emissions is significantly
540 more isotopically depleted than that of oceanic sources (Snider et al., 2015b). Nevertheless, our observation period is shorter than that of other studies, so the interannual trends determined here are more likely affected by year-to-year variability. Among all reported records, the decrease of $\delta^{15}\text{N}^{\text{bulk}}$ observed at Hateruma Island was the most up-to-date and smallest (-0.020-0.026‰ a⁻¹) (Toyoda et al., 2013). The authors argued that the smaller declining trend for $\delta^{15}\text{N}^{\text{bulk}}$ may be
545 explained by the recent increase in anthropogenic isotopic ratios particularly for agricultural N_2O emissions, although Ishijima et al. (2007) suggested a decline in both $\delta^{15}\text{N}^{\text{bulk}}$ and $\delta^{18}\text{O}$ in anthropogenic N_2O from 1952-1970 to 1970-2001 based on inverse modeling.

For the interannual trends observed at Jungfraujoch, it is noteworthy to point out that our observations covering a rather short period may lead to large uncertainties despite statistical
550 significance. The discrepancy found in the trends between the first and second phases indicates that variability of N_2O isotopic composition is likely to obscure interannual trends over shorter periods (Toyoda et al., 2013). Hence, extended time-series of isotopic measurements are needed to reevaluate, for example, the observed tendency of increase in $\delta^{18}\text{O}$ and $\delta^{15}\text{N}^{\text{SP}}$ at Jungfraujoch (Table 1; only significant during the first phase). For $\delta^{18}\text{O}$ of atmospheric N_2O , a generally



555 declining trend smaller than that of $\delta^{15}\text{N}^{\text{bulk}}$ has been indicated by a number of observations (Bernard et al., 2006; Ishijima et al., 2007; Park et al., 2012; Röckmann et al., 2003; Röckmann and Levin, 2005). This is expected as $\delta^{18}\text{O}$ of anthropogenic N_2O is not much different from that of the natural background, given that the oxygen atom in N_2O is largely derived from soil water and ambient oxygen during production (Rahn and Wahlen, 2000).

560 It is still a challenging task to disentangle interannual trends of $\delta^{15}\text{N}^{\text{SP}}\text{-N}_2\text{O}$ in the background atmosphere, due to limitations in analytical repeatability and precision (Harris et al., 2017; Mohn et al., 2014). Past results have reached inconsistent conclusions, showing positive (Bernard et al., 2006; Park et al., 2012; Prokopiou et al., 2017; Röckmann and Levin, 2005) or negative (Röckmann et al., 2003; Toyoda et al., 2013) trends of similar magnitude (Fig. 6). On the one
565 hand, the negative trend in $\delta^{15}\text{N}^{\text{SP}}$ could be explained by the significantly lower $\delta^{15}\text{N}^{\text{SP}}$ from anthropogenic sources (e.g. agricultural sources; Table S2) than of the tropospheric background (near 18‰; Fig. 6). On the other hand, Park et al. (2012) suggested that the increase of $\delta^{15}\text{N}^{\text{SP}}$ in the atmospheric N_2O may reflect a global increase in importance of the contribution by nitrification (high- $\delta^{15}\text{N}^{\text{SP}}$ process) to agricultural N_2O emissions. This is based on the
570 assumption that the growth of N_2O emissions is largely due to enhanced fertilizer application which promotes nitrification activity (Pérez et al., 2001; Tian et al., 2018). The observed mean increase rate of 0.02‰ a^{-1} for $\delta^{15}\text{N}^{\text{SP}}$ by Park et al. (2012) could then be translated into an increase of 13-23% for the relative amount of nitrification-derived N_2O between 1750 and 2005. However, this should be further evaluated with more frequent sampling (Park et al. (2012) only
575 sampled 1-6 times per year) and tested with isotopic measurements across the NH, where agricultural N_2O emissions are more dominant than in the SH. In addition, the strong seasonal pattern of $\delta^{15}\text{N}^{\text{SP}}$ at Jungfraujoch suggests that seasonal variations of $\delta^{15}\text{N}^{\text{SP}}$ in response to



climatic or source factors are crucial and must be taken into consideration for evaluating interannual $\delta^{15}\text{N}^{\text{SP}}$ trends.

580 **4.4 Simulated anthropogenic N₂O sources with the two-box model and comparison with other studies**

To further evaluate anthropogenic source signatures of N₂O isotopic composition, we applied a two-box model representing a well-mixed troposphere and stratosphere (Röckmann et al., 2003; Schilt et al., 2014; Sowers et al., 2002). The simulated trends of the N₂O mixing ratios and isotopic composition show a gradual increase in N₂O and decrease in the isotopic signatures (see Fig. 6), which agree with existing observations within the model uncertainty. However, this does not hold for individual studies considered separately. For example, the N₂O mixing ratios observed by Röckmann et al. (2003) and Prokopiou et al. (2017) would lead to a higher preindustrial N₂O compared to our model simulation, which is likely due to the uncertainty in the firm air records (Prokopiou et al., 2017).

We compared the anthropogenic isotopic signatures determined by our two-box model with other similar studies in Table 2. Our estimates generally lie within the ranges given in the earlier studies (Ishijima et al., 2007; Park et al., 2012; Prokopiou et al., 2017; Sowers et al., 2002; Toyoda et al., 2013). However, isotopic signatures of N₂O sources estimated for 2018 in this study are higher in $\delta^{15}\text{N}^{\text{bulk}}$ and $\delta^{18}\text{O}$ (by 4-8‰), and lower in $\delta^{15}\text{N}^{\text{SP}}$ (by 2-7‰) than model estimates for the early 2000s from two other studies from SH (Park et al., 2012; Prokopiou et al., 2017). Such differences in $\delta^{15}\text{N}^{\text{bulk}}$ and $\delta^{18}\text{O}$ could be related to interhemispheric differences, as the relative contributions of N₂O sources vary between the two hemispheres (Toyoda et al., 2013). Also, more interestingly, this could suggest a shift in the N₂O source isotopic signatures over the last few decades. For example, an increase of $\delta^{15}\text{N}^{\text{bulk}}$ in anthropogenic N₂O sources



over time may be attributed to growing contributions of other industrial/waste sources with high $\delta^{15}\text{N}^{\text{bulk}}$ (Prokopiou et al., 2017). In addition, if the assumption of increasing $\delta^{15}\text{N}^{\text{bulk}}$ and decreasing $\delta^{15}\text{N}^{\text{SP}}$ in anthropogenic N_2O sources over time holds, it points to a recently growing contribution of denitrification relative to nitrification, to the global atmospheric N_2O increase
605 (Sutka et al., 2006; Toyoda et al., 2013). This does not necessarily contradict Park et al. (2012) or Prokopiou et al. (2017), who proposed an increasing importance of nitrification for anthropogenic N_2O emissions based on the increasing $\delta^{15}\text{N}^{\text{SP}}$ trend since 1940, as the change in N_2O source processes in recent decades may instead reflect a stronger climate change feedback (Griffis et al., 2017; Xu-Ri et al., 2012).

610 Given the strong heterogeneity in source contributions to N_2O emissions around the globe (Saikawa et al., 2014), current two- and four-box model estimates based on observations at individual sites or regions are likely to reflect latitudinal or even interhemispheric differences in anthropogenic isotopic signatures. On the other hand, previous discussions of the model sensitivities by Röckmann et al. (2003) and Toyoda et al. (2013) have suggested that
615 anthropogenic isotopic values are most sensitive to the trends in tropospheric isotopic values as well as the relative difference in tropospheric isotopic values between present and preindustrial times. As shown in Figure 6, Park et al. (2012) observed lower $\delta^{15}\text{N}^{\text{bulk}}$ in the recent troposphere, and both Park et al. (2012) and Prokopiou et al. (2017) found a positive trend in $\delta^{15}\text{N}^{\text{SP}}$. These may help to explain some differences in anthropogenic source signatures between our and their
620 box model estimates.

Using an alternative bottom-up approach, we estimated the anthropogenic source isotopic signatures based on the N_2O emission inventory simulated for Jungfraujoch and published source isotopic signatures as summarized by Harris et al. (2017) (Table S2). The retrieved



anthropogenic isotopic signatures (Table 3) were largely in agreement with the isotopic signature
625 of agricultural soil emissions (Snider et al., 2015b; Wolf et al., 2015), indicating that this source
could explain more than 60% of the total N₂O emissions. However, the anthropogenic isotopic
signatures estimated by this approach were lower than the results from our two-box model (Table
2). In contrast, another similar bottom-up estimate based on the global N₂O emission inventory
(Toyoda et al., 2013) reported anthropogenic isotopic values that agree well with our box-model
630 results. This may be explained by the different isotopic signatures used to describe agricultural
N₂O emissions, as those values used for the bottom-up estimates by Toyoda et al. (2013) were
significantly lower (Toyoda et al., 2011) than those used in this study (Snider et al., 2015b; Wolf
et al., 2015). Such bottom-up estimation suggests that more isotopic measurements of the
background atmosphere from different regions, and better constraints on individual
635 anthropogenic (especially agricultural) N₂O isotopic signatures, are necessary for a better
representation of N₂O isotopic composition in atmospheric modeling studies.



5 Conclusions

With the recently developed laser spectroscopic technique coupled with a preconcentration device, we achieved good repeatability in measurements of N₂O isotopic composition from the background atmosphere at Jungfraujoch, Switzerland. This time-series covered a period of five years and showed a distinct seasonality, with $\delta^{15}\text{N}^{\text{bulk}}$ maxima and $\delta^{15}\text{N}^{\text{SP}}$ minima in late summer, associated with the lowest N₂O mixing ratios over the year. The seasonal fluctuation of $\delta^{15}\text{N}^{\text{bulk}}$ was associated with the stratosphere-troposphere exchange process, in agreement with other monitoring networks (Nevison et al., 2011), while the contrasting depletion of $\delta^{15}\text{N}^{\text{SP}}$ in later summer is possibly a combined result of STE and agricultural emissions, with the latter being more important. The analyses of air mass transport regimes together with the simulation of N₂O enhancements for Jungfraujoch supported our explanations and highlighted that the fluctuation between the free troposphere and local contributions dominated by soil emission drives the seasonality of $\delta^{15}\text{N}^{\text{SP}}$ and $\delta^{18}\text{O}$ as observed at Jungfraujoch.

We found statistically significant interannual trends for $\delta^{15}\text{N}^{\text{bulk}}$, which is expected as anthropogenic N₂O sources are characterized by low ¹⁵N abundance. For $\delta^{15}\text{N}^{\text{SP}}$ and $\delta^{18}\text{O}$, interannual trends were highly uncertain and possibly masked by higher-frequency temporal variation. Using a two-box model approach, we simulated the evolution of N₂O isotopic composition from preindustrial times to the present. This model suggests an overall decreasing trend for all isotopic species in conjunction with the atmospheric N₂O increase. The anthropogenic source signatures given by the model generally agreed with previous studies. However, these model results are still sensitive to the ranges and trends of the observed N₂O isotopic signatures in the present troposphere. In the future, more extended records of high-precision N₂O isotopic measurements and application of multiple-box modeling approaches



660 (Rigby et al., 2013) are necessary to account for the global N₂O budget and evolution of anthropogenic sources.



Data availability

Data for N₂O mixing ratios and isotopic composition of flask samples at Jungfraujoch could be found in the supplementary materials. *In situ* data for N₂O mixing ratios at Jungfraujoch are
665 available from World Data Centre for Greenhouse Gases (WMO-GAW; <https://gaw.kishou.go.jp>). Other data are available upon request through the corresponding author (longfei.yu@empa.ch).

Author contribution:

LY, EH and JM led and designed this study. LY, EH, SE conducted sample collection at
670 Jungfraujoch; LY and EH analyzed discrete samples at Empa; MS and CZ contributed *in situ* measurements of N₂O, NO_y, CO and O₃ at Jungfraujoch; LY, EH and SH performed data analyses for the time-series and conducted model simulations. LY wrote the main manuscript; EH, SH and JM were involved in the revisions of the manuscript and commenting. SE, MS, LE and CZ were also involved in scientific discussion and commenting on the manuscript.

675 Competing interests

The authors declare that they have no conflict of interest.

Acknowledgements

We are thankful to the research infrastructure provided by the High Altitude Research Stations Jungfraujoch and Gornergrat. We are grateful to the help from the custodians (Mr. and Mrs.
680 Fischer and Mr. and Mrs. Käser) at the research station of Jungfraujoch. We would like to thank Simon Wyss, Kerstin Zeyer, Patrik Zanchetta and Flurin Dietz for their support with the sample collection as well as laboratory assistance. The NABEL network is operated by Empa in collaboration with the Swiss Federal Office for the Environment. Prof. Sakae Toyoda and Prof.



Naohiro Yoshida from Tokyo Institute of Technology are acknowledged for their analyses of the
685 applied reference standards. This study was financially supported by the Swiss National Science
Foundation (grant number 200021_163075) and the Swiss contribution to the Integrated Carbon
Observation System (ICOS) Research Infrastructure (ICOS-CH). ICOS-CH is funded by the
Swiss National Science Foundation and in-house contributions. Longfei Yu was additionally
supported by the EMPAPOSTDOCS-II program, which receives funding from the European
690 Union's Horizon 2020 research and innovation program under the Marie Skłodowska-Curie
grant agreement number 754364.



References

- Appenzeller, C., Begert, M., Zenklusen, E. and Scherrer, S. C.: Monitoring climate at Jungfrauoch in the high Swiss Alpine region, *Sci. Total Environ.*, 391(2–3), 262–268, doi:10.1016/j.scitotenv.2007.10.005, 2008.
- Bernard, S., Röckmann, T., Kaiser, J., Barnola, J.-M., Fischer, H., Blunier, T. and Chappellaz, J.: Constraints on N₂O budget changes since pre-industrial time from new firm air and ice core isotope measurements, *Atmos. Chem. Phys. Discuss.*, 5(4), 7547–7575, doi:10.5194/acpd-5-7547-2005, 2006.
- Bourbonnais, A., Letscher, R. T., Bange, H. W., Échevin, V., Larkum, J., Mohn, J., Yoshida, N. and Altabet, M. A.: N₂O production and consumption from stable isotopic and concentration data in the Peruvian coastal upwelling system, *Global Biogeochem. Cycles*, 31(4), 678–698, doi:10.1002/2016GB005567, 2017.
- Buchmann, B., Hueglin, C., Reimann, S., Vollmer, M. K., Steinbacher, M. and Emmenegger, L.: Reactive gases, ozone depleting substances and greenhouse gases, in *From weather observations to atmospheric and climate sciences in Switzerland*, edited by S. Willemse and M. Furger, vdf Hochschulverlag AG., 2016.
- Bukowiecki, N., Weingartner, E., Gysel, M., Coen, M. C., Zieger, P., Herrmann, E., Steinbacher, M., Gäggeler, H. W. and Baltensperger, U.: A review of more than 20 years of aerosol observation at the high altitude research station Jungfrauoch, Switzerland (3580 m asl), *Aerosol Air Qual. Res.*, 16(3), 764–788, doi:10.4209/aaqr.2015.05.0305, 2016.
- Butterbach-Bahl, K., Baggs, E. M., Dannenmann, M., Kiese, R. and Zechmeister-Boltenstern, S.: Nitrous oxide emissions from soils: how well do we understand the processes and their controls?, *Philos. Trans. R. Soc. Lond. B. Biol. Sci.*, 368, 20130122, doi:10.1098/rstb.2013.0122, 2013.
- Decock, C. and Six, J.: How reliable is the intramolecular distribution of ¹⁵N in N₂O to source partition N₂O emitted from soil?, *Soil Biol. Biochem.*, 65(2), 114–127, doi:10.1016/j.soilbio.2013.05.012, 2013.
- Denk, T. R. A., Mohn, J., Decock, C., Lewicka-Szczebak, D., Harris, E., Butterbach-Bahl, K., Kiese, R. and Wolf, B.: The nitrogen cycle: A review of isotope effects and isotope modeling approaches, *Soil Biol. Biochem.*, 105, 121–137, doi:10.1016/j.soilbio.2016.11.015, 2017.
- Denk, T. R. A., Kraus, D., Kiese, R., Butterbach-Bahl, K. and Wolf, B.: Constraining N cycling in the ecosystem model LandscapeDNDC with the stable isotope model SIMONE, *Ecology*, 100(5), c02675, doi:10.1002/ecy.2675, 2019.
- Fowler, D., Steadman, C. E., Stevenson, D., Coyle, M., Rees, R. M., Skiba, U. M., Sutton, M. a., Cape, J. N., Dore, a. J., Vieno, M., Simpson, D., Zaehle, S., Stocker, B. D., Rinaldi, M., Facchini, M. C., Flechard, C. R., Nemitz, E., Twigg, M., Erisman, J. W. and Galloway, J. N.: Effects of global change during the 21st century on the nitrogen cycle, *Atmos. Chem. Phys. Discuss.*, 15(2), 1747–1868, doi:10.5194/acpd-15-1747-2015, 2015.
- Fujii, A., Toyoda, S., Yoshida, O., Watanabe, S., Sasaki, K. and Yoshida, N.: Distribution of nitrous oxide dissolved in water masses in the eastern subtropical North Pacific and its origin inferred from isotopomer analysis, *J. Oceanogr.*, 69(2), 147–157, doi:10.1007/s10872-012-0162-4, 2013.
- Griffis, T. J., Chen, Z., Baker, J. M., Wood, J. D., Millet, D. B., Lee, X., Venterea, R. T. and Turner, P. A.: Nitrous oxide emissions are enhanced in a warmer and wetter world, *Proc. Natl. Acad. Sci.*, 201704552, doi:10.1073/pnas.1704552114, 2017.
- Hall, B. D., Dutton, G. S. and Elkins, J. W.: The NOAA nitrous oxide standard scale for atmospheric observations, *J. Geophys. Res. Atmos.*, 112(9), 1–9, doi:10.1029/2006JD007954, 2007.



- Harris, E., Ibraim, E., Henne, S., Hüglin, C., Zellweger, C., Tuzson, B., Emmenegger, L. and Mohn, J.: Tracking nitrous oxide emission processes at a suburban site with semicontinuous, in situ measurements of isotopic composition, *J. Geophys. Res. Atmos.*, 122, 1850–1870, doi:10.1002/2016JD025906, 2017.
- 740 Harris, E. J., Nelson, D. D., Olsewski, W., Zahniser, M., Potter, E., Mcmanus, B. J., Whitehill, A., Prinn, R. G., Ono, S. and Harris, E.: Development of a spectroscopic technique for continuous online monitoring of oxygen and site-specific nitrogen isotopic com, *Anal. Chem.*, 86(3), 1726–1734, 2014.
- Heil, J., Wolf, B., Brüggemann, N., Emmenegger, L., Tuzson, B., Vereecken, H. and Mohn, J.: Site-specific ^{15}N isotopic signatures of abiotically produced N_2O , *Geochim. Cosmochim. Acta*, 139, 72–82, doi:10.1016/j.gca.2014.04.037, 2014.
- 745 Henne, S., Brunner, D., Folini, D., Solberg, S., Klausen, J. and Buchmann, B.: Assessment of parameters describing representativeness of air quality in-situ measurement sites, *Atmos. Chem. Phys.*, 10(8), 3561–3581, doi:10.5194/acp-10-3561-2010, 2010.
- Henne, S., Brunner, D., Oney, B., Leuenberger, M., Eugster, W., Bamberger, I., Meinhardt, F., Steinbacher, M. and Emmenegger, L.: Validation of the Swiss methane emission inventory by atmospheric observations and inverse modelling, *Atmos. Chem. Phys.*, 16(6), 3683–3710, doi:10.5194/acp-16-3683-2016, 2016.
- Henne, S., Mohn, J. and Brunner, D.: Quantification of Swiss nitrous oxide emissions through atmospheric observations and inverse modelling, Final Report, Project of FOEN, 2019.
- 755 Herrmann, E., Weingartner, E., Henne, S., Vuilleumier, L., Bukowiecki, N., Steinbacher, M., Conen, F., Coen, M. C., Hammer, E., Juranyi, Z., Baltensperger, U. and Gysel, M.: Analysis of long-term aerosol size distribution data from Jungfraujoch with emphasis on free tropospheric conditions, cloud influence, and air mass transport, *J. Geophys. Res. Atmos.*, 120, 1751–1762, doi:10.1002/2015JD023660, 2015.
- 760 Ibraim, E., Wolf, B., Harris, E., Gasche, R., Wei, J., Yu, L., Kiese, R., Eggleston, S., Butterbach-Bahl, K., Zeeman, M., Tuzson, B., Emmenegger, L., Six, J., Henne, S. and Mohn, J.: Attribution of N_2O sources in a grassland soil with laser spectroscopy based isotopocule analysis, *Biogeosciences*, 16, 3247–3266, doi.org/10.5194/bg-16-3247-2019, 2019.
- 765 Ishijima, K., Sugawara, S., Kawamura, K., Hashida, G., Morimoto, S., Murayama, S., Aoki, S. and Nakazawa, T.: Temporal variations of the atmospheric nitrous oxide concentration and its $\delta^{15}\text{N}$ and $\delta^{18}\text{O}$ for the latter half of the 20th century reconstructed from firm air analyses, *J. Geophys. Res. Atmos.*, 112(3), doi:10.1029/2006JD007208, 2007.
- Janssens-Maenhout, G., Crippa, M., Guizzardi, D., Muntean, M., Schaaf, E., Dentener, F., Bergamaschi, P., Pagliari, V., Olivier, J., Peters, J., van Aardenne, J., Monni, S., Doering, U., Petrescu, R., Solazzo, E. and Oreggioni, G.: EDGAR v4.3.2 Global Atlas of the three major Greenhouse Gas Emissions for the period 1970–2012, *Earth Syst. Sci. Data Discuss.*, 2010, 1–52, doi:10.5194/essd-2018-164, 2019.
- 770 Jiang, X., Ku, W. L., Shia, R. L., Li, Q., Elkins, J. W., Prinn, R. G. and Yung, Y. L.: Seasonal cycle of N_2O : Analysis of data, *Global Biogeochem. Cycles*, 21, GB1006, doi:10.1029/2006GB002691, 2007.
- JMA and WMO: World Meteorological Organization - Global Atmosphere Watch - World Data Centre for Greenhouse Gases, Data Summary, No. 42, 101 p., [online] Available from: <https://gaw.kishou.go.jp/static/publications/summary/sum42/sum42.pdf>, 2018.
- 775 Kaiser, J., Röckmann, T. and Brenninkmeijer, C. A. M.: Complete and accurate mass spectrometric isotope analysis of tropospheric nitrous oxide, *J. Geophys. Res. Atmos.*, 108, 4476, doi:10.1029/2003JD003613, D15.
- 780 Keller, C. A., Hill, M., Vollmer, M. K., Henne, S., Brunner, D., Reimann, S., O’Doherty, S., Arduini, J., Maione, M., Ferenczi, Z., Haszpra, L., Manning, A. J. and Peter, T.: European emissions of halogenated greenhouse gases inferred from atmospheric measurements, *Environ. Sci. Technol.*, 46(1), 217–225,



- doi:10.1021/es202453j, 2012.
- Kim, K.-R. and Craig, H.: Nitrogen-15 and Oxygen-18 Characteristics of Nitrous Oxide: A Global Perspective, *Science*, 262, 1855–1857, 1993.
- 785 Lebegue, B., Schmidt, M., Ramonet, M., Wastine, B., Yver Kwok, C., Laurent, O., Belviso, S., Guemri, A., Philippon, C., Smith, J. and Conil, S.: Comparison of nitrous oxide (N₂O) analyzers for high-precision measurements of atmospheric mole fractions, *Atmos. Meas. Tech.*, 9(3), 1221–1238, doi:10.5194/amt-9-1221-2016, 2016.
- 790 Logan, J. A., Staehelin, J., Megretskaia, I. A., Cammas, J. P., Thouret, V., Claude, H., De Backer, H., Steinbacher, M., Scheel, H. E., Stbi, R., Frhlich, M. and Derwent, R.: Changes in ozone over Europe: Analysis of ozone measurements from sondes, regular aircraft (MOZAIC) and alpine surface sites, *J. Geophys. Res. Atmos.*, 117(9), 1–23, doi:10.1029/2011JD016952, 2012.
- Mohn, J., Guggenheim, C., Tuzson, B., Vollmer, M. K., Toyoda, S., Yoshida, N. and Emmenegger, L.: A liquid nitrogen-free preconcentration unit for measurements of ambient N₂O isotopomers by QCLAS, *Atmos. Meas. Tech.*, 3(3), 609–618, doi:10.5194/amt-3-609-2010, 2010.
- 795 Mohn, J., Tuzson, B., Manninen, A., Yoshida, N., Toyoda, S., Brand, W. A. and Emmenegger, L.: Site selective real-time measurements of atmospheric N₂O isotopomers by laser spectroscopy, *Atmos. Meas. Tech.*, 5(7), 1601–1609, doi:10.5194/amt-5-1601-2012, 2012.
- 800 Mohn, J., Wolf, B., Toyoda, S., Lin, C. T., Liang, M. C., Brüggemann, N., Wissel, H., Steiker, A. E., Dyckmans, J., Szwec, L., Ostrom, N. E., Casciotti, K. L., Forbes, M., Giesemann, A., Well, R., Doucett, R. R., Yarnes, C. T., Ridley, A. R., Kaiser, J. and Yoshida, N.: Interlaboratory assessment of nitrous oxide isotopomer analysis by isotope ratio mass spectrometry and laser spectroscopy: Current status and perspectives, *Rapid Commun. Mass Spectrom.*, 28(18), 1995–2007, doi:10.1002/rcm.6982, 2014.
- 805 Nevison, C. D., Keeling, R. F., Weiss, R. F., Popp, B. N., Jin, X., Fraser, P. J., Porter, L. W. and Hess, P. G.: Southern Ocean ventilation inferred from seasonal cycles of atmospheric N₂O and O₂/N₂ at Cape Grim, Tasmania, *Tellus, Ser. B Chem. Phys. Meteorol.*, 57(3), 218–229, doi:10.1111/j.1600-0889.2005.00143.x, 2005.
- 810 Nevison, C. D., Dlugokencky, E., Dutton, G., Elkins, J. W., Fraser, P., Hall, B., Krummel, P. B., Langenfelds, R. L., O’Doherty, S., Prinn, R. G., Steele, L. P. and Weiss, R. F.: Exploring causes of interannual variability in the seasonal cycles of tropospheric nitrous oxide, *Atmos. Chem. Phys.*, 11(8), 3713–3730, doi:10.5194/acp-11-3713-2011, 2011.
- Ogawa, M. and Yoshida, N.: Intramolecular distribution of stable nitrogen and oxygen isotopes of nitrous oxide emitted during coal combustion, *Chemosphere*, 61(6), 877–887, doi:10.1016/j.chemosphere.2005.04.096, 2005.
- 815 Ostrom, N. E., Gandhi, H., Coplen, T. B., Toyoda, S., Böhlke, J. K., Brand, W. A., Casciotti, K. L., Dyckmans, J., Giesemann, A., Mohn, J., Well, R., Yu, L. and Yoshida, N.: Preliminary assessment of stable nitrogen and oxygen isotopic composition of USGS51 and USGS52 nitrous oxide reference gases and perspectives on calibration needs, *Rapid Commun. Mass Spectrom.*, 32(15), 1207–1214, doi:10.1002/rcm.8157, 2018.
- 820 Pandey Deolal, S., Brunner, D., Steinbacher, M., Weers, U. and Staehelin, J.: Long-term in situ measurements of NO_x and NO_y at Jungfraujoch 1998–2009: Time series analysis and evaluation, *Atmos. Chem. Phys.*, 12(5), 2551–2566, doi:10.5194/acp-12-2551-2012, 2012.
- 825 Park, S., Croteau, P., Boering, K. A., Etheridge, D. M., Ferretti, D., Fraser, P. J., Kim, K.-R., Krummel, P. B., Langenfelds, R. L., van Ommen, T. D., Steele, L. P. and Trudinger, C. M.: Trends and seasonal cycles in the isotopic composition of nitrous oxide since 1940, *Nat. Geosci.*, 5(4), 261–265, doi:10.1038/ngeo1421, 2012.



- Pérez, T., Trumbore, S. E., Tyler, S. C., Matson, P. A., I., O.-M., Rahn, T. and Griffiths, D. W. T.: Identifying the agricultural imprint on the global N₂O budget using stable isotopes, *J. Geophys. Res.*, 106, 9869–9878, doi:10.1179/1607845413y.0000000087, 2001.
- 830 Prather, M. J., Hsu, J., Deluca, N. M., Jackman, C. H., Oman, L. D., Douglass, A. R., Fleming, E. L., Strahan, S. E., Steenrod, S. D., Søvde, O. A., Isaksen, I. S. A., Froidevaux, L. and Funke, B.: Measuring and modeling the lifetime of nitrous oxide including its variability Michael, *J. Geophys. Res. Atmos.*, 120, 5693–5705, doi:10.1002/2015JD023267. Received, 2015.
- 835 Prinn, R. G., Weiss, R. F., Arduini, J., Arnold, T., Dewitt, H. L., Fraser, P. J., Ganesan, A. L., Gasore, J., Harth, C. M., Hermansen, O., Kim, J., Krummel, P. B., Li, S., Loh, Z. M., Lunder, C. R. and Maione, M.: History of chemically and radiatively important atmospheric gases from the Advanced Global Atmospheric Gases Experiment (AGAGE), *Earth Syst. Sci. Data*, 10, 985–1018, 2018.
- 840 Prokopiou, M., Martinerie, P., Sapart, C. J., Witrant, E., Monteil, G. A., Ishijima, K., Bernard, S., Kaiser, J., Levin, I., Sowers, T., Blunier, T., Etheridge, D., Dlugokencky, E., van de Wal, R. S. W. and Röckmann, T.: Constraining N₂O emissions since 1940 using firm air isotope measurements in both hemispheres, *Atmos. Chem. Phys.*, 2011(June), 1–50, doi:10.5194/acp-2016-487, 2017.
- Prokopiou, M., Sapart, C. J., Rosen, J., Sperlich, P., Blunier, T., Brook, E., van de Wal, R. S. W. and Röckmann, T.: Changes in the Isotopic Signature of Atmospheric Nitrous Oxide and Its Global Average Source During the Last Three Millennia, *J. Geophys. Res. Atmos.*, 1–17, doi:10.1029/2018JD029008, 2018.
- 845 Rahn, T. and Wahlen, M.: A reassessment of the global isotopic budget of atmospheric nitrous oxide, *Global Biogeochem. Cycles*, 14(2), 537–543, doi:10.1029/1999GB900070, 2000.
- Ravishankara, A. R., Daniel, J. S. and Portmann, R. W.: Nitrous oxide (N₂O): the dominant ozone-depleting substance emitted in the 21st century., *Science*, 326(5949), 123–5, doi:10.1126/science.1176985, 2009.
- 850 Reay, D. S., Davidson, E. a., Smith, K. a., Smith, P., Melillo, J. M., Dentener, F. and Crutzen, P. J.: Global agriculture and nitrous oxide emissions, *Nat. Clim. Chang.*, 2(6), 410–416, doi:10.1038/nclimate1458, 2012.
- 855 Reimann, S., Vollmer, M. K., Folini, D., Steinbacher, M., Hill, M., Buchmann, B., Zander, R. and Mahieu, E.: Observations of long-lived anthropogenic halocarbons at the high-Alpine site of Jungfraujoch (Switzerland) for assessment of trends and European sources, *Sci. Total Environ.*, 391(2–3), 224–231, doi:10.1016/j.scitotenv.2007.10.022, 2008.
- 860 Rigby, M., Prinn, R. G., O’Doherty, S., Montzka, S. A., McCulloch, A., Harth, C. M., Mühle, J., Salameh, P. K., Weiss, R. F., Young, D., Simmonds, P. G., Hall, B. D., Dutton, G. S., Nance, D., Mondeel, D. J., Elkins, J. W., Krummel, P. B., Steele, L. P. and Fraser, P. J.: Re-evaluation of the lifetimes of the major CFCs and CH₃CCl₃ using atmospheric trends, *Atmos. Chem. Phys.*, 13(5), 2691–2702, doi:10.5194/acp-13-2691-2013, 2013.
- Röckmann, T., Kaiser, J. and Brenninkmeijer, C. A. M.: The isotopic fingerprint of the pre-industrial and the anthropogenic N₂O source, *Atmos. Chem. Phys.*, (3), 315–323, 2003.
- 865 Röckmann, T. and Levin, I.: High-precision determination of the changing isotopic composition of atmospheric N₂O from 1990 to 2002, *J. Geophys. Res. Atmos.*, 110(21), 1–8, doi:10.1029/2005JD006066, 2005.
- 870 Saikawa, E., Prinn, R. G., Dlugokencky, E., Ishijima, K., Dutton, G. S., Hall, B. D., Langenfelds, R., Tohjima, Y., Machida, T., Manizza, M., Rigby, M., O’Doherty, S., Patra, P. K., Harth, C. M., Weiss, R. F., Krummel, P. B., Van Der Schoot, M., Fraser, P. J., Steele, L. P., Aoki, S., Nakazawa, T. and Elkins, J. W.: Global and regional emissions estimates for N₂O, *Atmos. Chem. Phys.*, 14(9), 4617–4641,



- doi:10.5194/acp-14-4617-2014, 2014.
- Schibig, M. F., Steinbacher, M., Buchmann, B., Van Der Laan-Luijkx, I. T., Van Der Laan, S., Ranjan, S. and Leuenberger, M. C.: Comparison of continuous in situ CO₂ observations at Jungfraujoch using two different measurement techniques, *Atmos. Meas. Tech.*, 8(1), 57–68, doi:10.5194/amt-8-57-2015, 2015.
- 875 Schilt, A., Brook, E. J., Bauska, T. K., Baggenstos, D., Fischer, H., Joos, F., Petrenko, V. V., Schaefer, H., Schmitt, J., Severinghaus, J. P., Spahni, R. and Stocker, T. F.: Isotopic constraints on marine and terrestrial N₂O emissions during the last deglaciation, *Nature*, 516(7530), 234–237, doi:10.1038/nature13971, 2014.
- 880 Sepúlveda, E., Schneider, M., Hase, F., Barthlott, S., Dubravica, D., García, O. E., Gomez-Pelaez, A., González, Y., Guerra, J. C., Gisi, M., Kohlhepp, R., Dohe, S., Blumenstock, T., Strong, K., Weaver, D., Palm, N., Sadeghi, A., Deutscher, N. M., Warneke, T., Notholt, J., Jones, N., Griffith, D. W. T., Smale, D., Brailsford, G. W., Robinson, J., Meinhardt, F., Steinbacher, M., Aalto, T. and Worthy, D.: Tropospheric CH₄ signals as observed by NDACC FTIR at globally distributed sites and comparison to GAW surface in situ measurements, *Atmos. Meas. Tech.*, 7(7), 2337–2360, doi:10.5194/amt-7-2337-2014, 2014.
- 885 Snider, D., Thompson, K., Wagner-Riddle, C., Spoelstra, J. and Dunfield, K.: Molecular techniques and stable isotope ratios at natural abundance give complementary inferences about N₂O production pathways in an agricultural soil following a rainfall event, *Soil Biol. Biochem.*, 88, 197–213, doi:10.1016/j.soilbio.2015.05.021, 2015a.
- 890 Snider, D. M., Venkiteswaran, J. J., Schiff, S. L. and Spoelstra, J.: From the ground up: Global nitrous oxide sources are constrained by stable isotope values, *PLoS One*, 10(3), 1–19, doi:10.1371/journal.pone.0118954, 2015b.
- Sowers, T., Rodebaugh, A., Yoshida, N. and Toyoda, S.: Extending records of the isotopic composition of atmospheric N₂O back to 1800 A.D. from air trapped in snow at the South Pole and the Greenland Ice Sheet Project II ice core, *Global Biogeochem. Cycles*, 16(4), 1–10, doi:10.1029/2002GB001911, 2002.
- 895 Stohl, A., Forster, C., Frank, A., Seibert, P. and Wotawa, G.: Technical note: The Lagrangian particle dispersion model FLEXPART version 6.2, *Atmos. Chem. Phys.*, 5, 2461–2474, doi:10.3390/atmos9020076, 2005.
- 900 Sturm, P., Tuzson, B., Henne, S. and Emmenegger, L.: Tracking isotopic signatures of CO₂ at the high altitude site Jungfraujoch with laser spectroscopy: Analytical improvements and representative results, *Atmos. Meas. Tech.*, 6(7), 1659–1671, doi:10.5194/amt-6-1659-2013, 2013.
- 905 Sutka, R. L., Ostrom, N. E., Ostrom, P. H., Breznak, J. a, Pitt, a J., Li, F. and Gandhi, H.: Distinguishing Nitrous Oxide Production from Nitrification and Denitrification on the Basis of Isotopomer Abundances Distinguishing Nitrous Oxide Production from Nitrification and Denitrification on the Basis of Isotopomer Abundances, *Appl. Environ. Microbiol.*, 72(1), 638–644, doi:10.1128/AEM.72.1.638, 2006.
- Tarasova, O. A., Senik, I. A., Sosonkin, M. G., Cui, J., Staehelin, J. and Péévo, A. S. H.: Surface ozone at the Caucasian site Kislovodsk High Mountain Station and the Swiss Alpine site Jungfraujoch: Data analysis and trends (1990-2006), *Atmos. Chem. Phys.*, 9(12), 4157–4175, doi:10.5194/acp-9-4157-2009, 2009.
- 910 Team, R. C.: A language and environment for statistical computing. R Foundation for statistical computing, 2015; Vienna, Austria, 2016.
- 915 Thompson, R. L., Patra, P. K., Ishijima, K., Saikawa, E., Corazza, M., Karstens, U., Wilson, C., Bergamaschi, P., Dlugokencky, E., Sweeney, C., Prinn, R. G., Weiss, R. F., O'Doherty, S., Fraser, P. J., Steele, L. P., Krummel, P. B., Saunois, M., Chipperfield, M. and Bousquet, P.: TransCom N₂O model inter-comparison-Part 1: Assessing the influence of transport and surface fluxes on tropospheric N₂O



- variability, *Atmos. Chem. Phys.*, 14(8), 4349–4368, doi:10.5194/acp-14-4349-2014, 2014a.
- Thompson, R. L., Ishijima, K., Saikawa, E., Corazza, M., Karstens, U., Patra, P. K., Bergamaschi, P., Chevallier, F., Dlugokencky, E., Prinn, R. G., Weiss, R. F., O'Doherty, S., Fraser, P. J., Steele, L. P., Krummel, P. B., Vermeulen, A., Tohjima, Y., Jordan, A., Haszpra, L., Steinbacher, M., Van Der Laan, S.,
920 Aalto, T., Meinhardt, F., Popa, M. E., Moncrieff, J. and Bousquet, P.: TransCom N₂O model inter-comparison - Part 2: Atmospheric inversion estimates of N₂O emissions, *Atmos. Chem. Phys.*, 14(12), 6177–6194, doi:10.5194/acp-14-6177-2014, 2014b.
- Thoning, K. W., Tans, P. P. and Komhyr, W. D.: Atmospheric carbon dioxide at Mauna Loa Observatory: 2. Analysis of the NOAA GMCC data, 1974-1985, *J. Geophys. Res.*, 94(D6), 8549–8565,
925 doi:10.1029/jd094id06p08549, 1989.
- Tian, H., Yang, J., Xu, R., Lu, C., Canadell, J., Davidson, E. A., Jackson, R., Arneeth, A., Chang, J., Ciais, P., Gerber, S., Ito, A., Joos, F., Lienert, S., Messina, P., Olin, S., Pan, S., Peng, C., Saikawa, E., Thompson, R., Vuichard, N., Winiwarter, W., Zaehle, S. and Zhang, B.: Global soil nitrous oxide emissions since the preindustrial era estimated by an ensemble of terrestrial biosphere models: Magnitude,
930 attribution, and uncertainty, *Glob. Chang. Biol.*, 25(2), 640–659, doi:10.1111/gcb.14514, 2018.
- Toyoda, S., Yoshida, N., Urabe, T., Aoki, S., Nakazawa, T., Sugawara, S. and Honda, H.: Fractionation of N₂O isotopomers in the stratosphere, *J. Geophys. Res.*, 106(D7), 7515, doi:10.1029/2000JD900680, 2001.
- Toyoda, S., Yamamoto, S., Arai, S., Nara, H., Yoshida, N., Kashiwakura, K. and Akiyama, K.:
935 Isotopomeric characterization of N₂O produced, consumed, and emitted by automobiles, rapid comm, 22, 603–612, doi:10.1002/rcm, 2008.
- Toyoda, S., Yano, M., Nishimura, S., Akiyama, H., Hayakawa, A., Koba, K., Sudo, S., Yagi, K., Makabe, A., Tobar, Y., Ogawa, N. O., Ohkouchi, N., Yamada, K. and Yoshida, N.: Characterization and production and consumption processes of N₂O emitted from temperate agricultural soils determined via isotopomer ratio analysis, *Global Biogeochem. Cycles*, 25(2), 1–17, doi:10.1029/2009GB003769, 2011.
- Toyoda, S., Kuroki, N., Yoshida, N., Ishijima, K., Tohjima, Y. and Machida, T.: Decadal time series of tropospheric abundance of N₂O isotopomers and isotopologues in the Northern Hemisphere obtained by the long-term observation at Hateruma Island, Japan, *J. Geophys. Res. Atmos.*, 118(8), 3369–3381, doi:10.1002/jgrd.50221, 2013.
- 945 Toyoda, S., Yoshida, N. and Koba, K.: Isotopocule analysis of biologically produced nitrous oxide in various environments, *Mass Spectrom. Rev.*, (36), 135–160, doi:doi:10.1002/mas.21459, 2017.
- Tuzson, B., Henne, S., Brunner, D., Steinbacher, M., Mohn, J., Buchmann, B. and Emmenegger, L.: Continuous isotopic composition measurements of tropospheric CO₂ at Jungfraujoch (3580 m a.s.l.), Switzerland: Real-time observation of regional pollution events, *Atmos. Chem. Phys.*, 11(4), 1685–1696,
950 doi:10.5194/acp-11-1685-2011, 2011.
- WMO: WMO Greenhouse Gas Bulletin., 2018.
- Wolf, B., Merbold, L., Decock, C., Tuzson, B., Harris, E., Six, J., Emmenegger, L. and Mohn, J.: First on-line isotopic characterization of N₂O above intensively managed grassland, *Biogeosciences*, 12(8), 2517–2531, doi:10.5194/bg-12-2517-2015, 2015.
- 955 Xu-Ri, Prentice, I. C., Spahni, R. and Niu, H. S.: Modelling terrestrial nitrous oxide emissions and implications for climate feedback, *New Phytol.*, 196(2), 472–488, doi:10.1111/j.1469-8137.2012.04269.x, 2012.
- Yoshida, N. and Toyoda, S.: Constraining the atmospheric N₂O budget from intramolecular site preference in N₂O isotopomers, *Nature*, 405(6784), 330–4, doi:10.1038/35012558, 2000.



- 960 Yuan, Y., Ries, L., Petermeier, H., Steinbacher, M., Gómez-Pelaéz, A. J., Leuenberger, M. C., Schumacher, M., Trickl, T., Couret, C., Meinhardt, F. and Menzel, A.: Adaptive selection of diurnal minimum variation: A statistical strategy to obtain representative atmospheric CO₂ data and its application to European elevated mountain stations, *Atmos. Meas. Tech.*, 11(3), 1501–1514, doi:10.5194/amt-11-1501-2018, 2018.
- 965 Yung, Y. L. and Miller, C. E.: Isotopic fractionation of stratospheric nitrous oxide, *Science*, 278(5344), 1778–1780, doi:10.1126/science.278.5344.1778, 1997.
- Zellweger, C., Forrer, J., Hofer, P., Nyeki, S., Schwarzenbach, B., Weingartner, E., Ammann, M. and Baltensperger, U.: Partitioning of reactive nitrogen (NO_y) and dependence on meteorological conditions in the lower free troposphere, *Atmos. Chem. Phys.*, 3(3), 779–796, doi:10.5194/acp-3-779-2003, 2003.
- 970 Zellweger, C., Hüglin, C., Klausen, J., Steinbacher, M., Vollmer, M. and Buchmann, B.: Inter-comparison of four different carbon monoxide measurement techniques and evaluation of the long-term carbon monoxide time series of Jungfraujoch, *Atmos. Chem. Phys.*, 9(11), 3491–3503, doi:10.5194/acp-9-3491-2009, 2009.



Table 1 Trends of atmospheric $\delta^{15}\text{N}^{\text{bulk}}$, $\delta^{15}\text{N}^{\text{SP}}$ and $\delta^{18}\text{O}$ at Jungfraujoch determined using discrete measurements between April 2014 and December 2018. The trends are determined for the whole dataset, the dataset filtered for free troposphere (removing data points with significant influence from planetary boundary layer) and the second-phase dataset with bi-weekly measurements (August 2016 to December 2018).

	$\delta^{15}\text{N}^{\text{bulk}}$ (‰ a ⁻¹)		$\delta^{15}\text{N}^{\text{SP}}$ (‰ a ⁻¹)		$\delta^{18}\text{O}$ (‰ a ⁻¹)	
	Raw	Deseasonalized	Raw	Deseasonalized	Raw	Deseasonalized
Whole dataset	-0.059±0.012*	-0.052±0.012*	0.069±0.029	0.065±0.027	0.020±0.011	0.019±0.011
Free troposphere	-0.060±0.014*	-0.054±0.013*	0.054±0.034	0.036±0.030	0.024±0.013	0.019±0.011
First phase (Apr. 2014-Feb. 2016)	-0.036±0.038	-0.041±0.035	0.449±0.100*	0.314±0.082*	0.238±0.029*	0.207±0.026*
Second phase (Aug. 2016-Dec. 2018)	-0.105±0.049	-0.130±0.045*	0.028±0.067	-0.007±0.066	-0.007±0.042	-0.001±0.040

* Indicate significance of linear regression.



980 **Table 2** Results of the two-box model simulations and selected literature values for comparison.

Variable	Anthropogenic source						
	This study	RMSE	Sowers et al. (2002) ^a	Ishijima et al. (2007) ^b	Toyoda et al. (2013) ^c	Park et al. (2012) ^d	Prokopiou et al. (2017) ^e
Air Sample Origin	NH [†] 2014-2018		FA, IC [†] 1745-1995	FA [†] 1960-2001	NH [†] 1999-2010	SH, FA [†] 1940-2005	FA [†] 1940-2008
α *	0.0154±0.004	0.65 nmol mol ⁻¹	0.0111 to 0.0128				
$F_{\text{anth},2018}$ (TgN y ⁻¹)	8.6±0.6	NA	4.2 to 5.7		5.5	6.6	5.4±1.7
$\delta^{15}\text{N}^{\text{bulk}}$ (‰)	-8.6±4	0.23	-7 to -13	-11.6	-9.84	-15.6±1.2	-18.2±2.6
$\delta^{18}\text{O}$ (‰)	34.8±3	0.22	17 to 26		35.95	32.0±1.3	27.2±2.6
$\delta^{15}\text{N}^{\text{SP}}$ (‰)	10.7±4	0.50			8.52	13.1±9.4	18.0±8.6

[†] NH and SH: surface atmosphere from the Northern and Southern Hemisphere, respectively; FA: firm air; IC: ice core air.

* “Value” is the dimensionless constant α describing the exponential increase in the anthropogenic flux

[‡] RMSE refers to root mean square error. It is in nmol mol⁻¹ for α , referring to the present day

985 tropospheric mixing ratio for N₂O. For source isotopic values, RMSE is in the unit of ‰.

^a Estimates are for 1995

^b Estimate is for 2000, for $\delta^{18}\text{O}$ calibration is not comparable

^c Estimates are for 2012 using the “Base” scenario

^d Estimates are for 2005

990 ^e δ_{anth} values are averaged values for the period of 1940-2008.



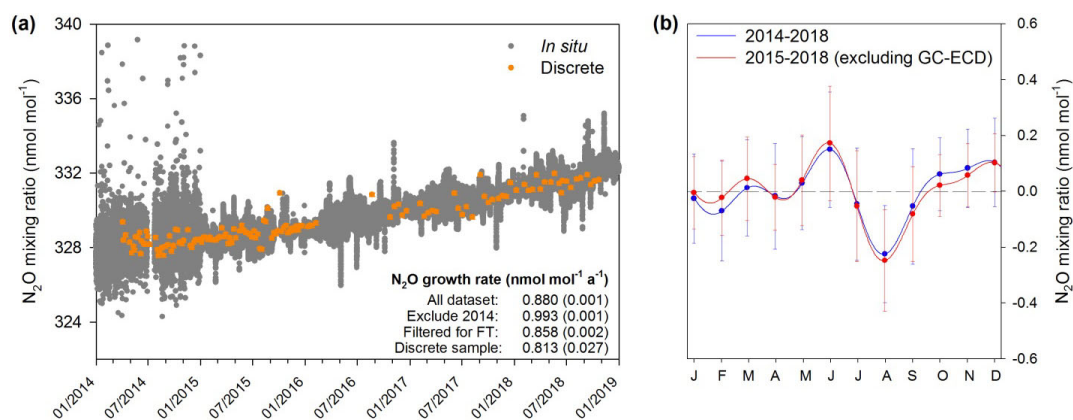
Table 3 Isotopic signatures for the overall, anthropogenic and major N₂O sources contributing to N₂O variations at Jungfrauoch. Source signatures were estimated based on a “bottom-up” approach, with literature-derived isotopic signatures and fluxes for variable sources under the Swiss Meteotest emission inventory.

	Emission inventory (%)	$\delta^{15}\text{N}^{\text{bulk}}$ (‰)	$\delta^{15}\text{N}^{\text{SP}}$ (‰)	$\delta^{18}\text{O}$ (‰)	Reference
Overall source	100	-15.8 (6.2)	7.3 (3.9)	29.4 (5.5)	-
Anthropogenic source	89.4	-15.6 (6.3)	7.4 (4.0)	29.5 (5.7)	-
Agricultural emission	61.5	-17.8 (5.7)	7.2 (3.8)	29.0 (3.7)	Snider et al. (2015) Wolf et al. (2015)
Manure management	7.4	-17.5 (6.2)	6.5 (4.1)	23.9 (3.8)	Maeda et al. (2010)
Waste*	7.2	-11.5 (12.6)	10.4 (5.7)	31.3 (14.0)	Ogawa and Yoshida (2005) Snider et al. (2015)
Natural emission	10.9	-17.8 (5.7)	7.2 (3.8)	29.0 (3.7)	Snider et al. (2015) Wolf et al. (2015)

995 * “Waste” sources consist of both wastewater treatment and agricultural waste burning (biomass burning).

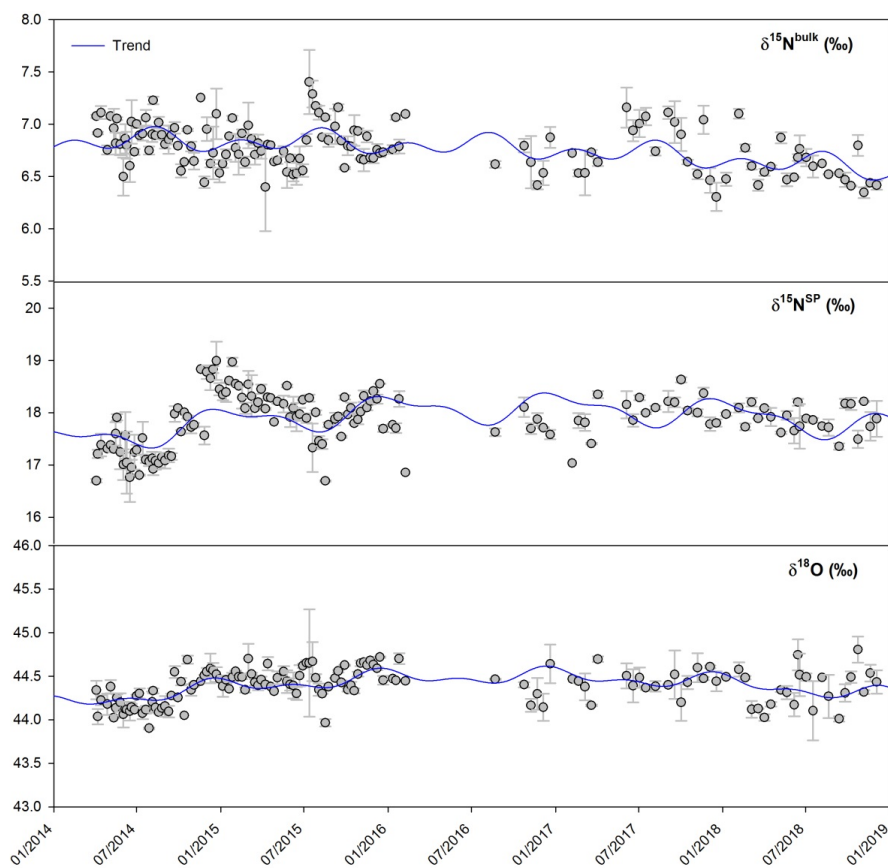


Figures

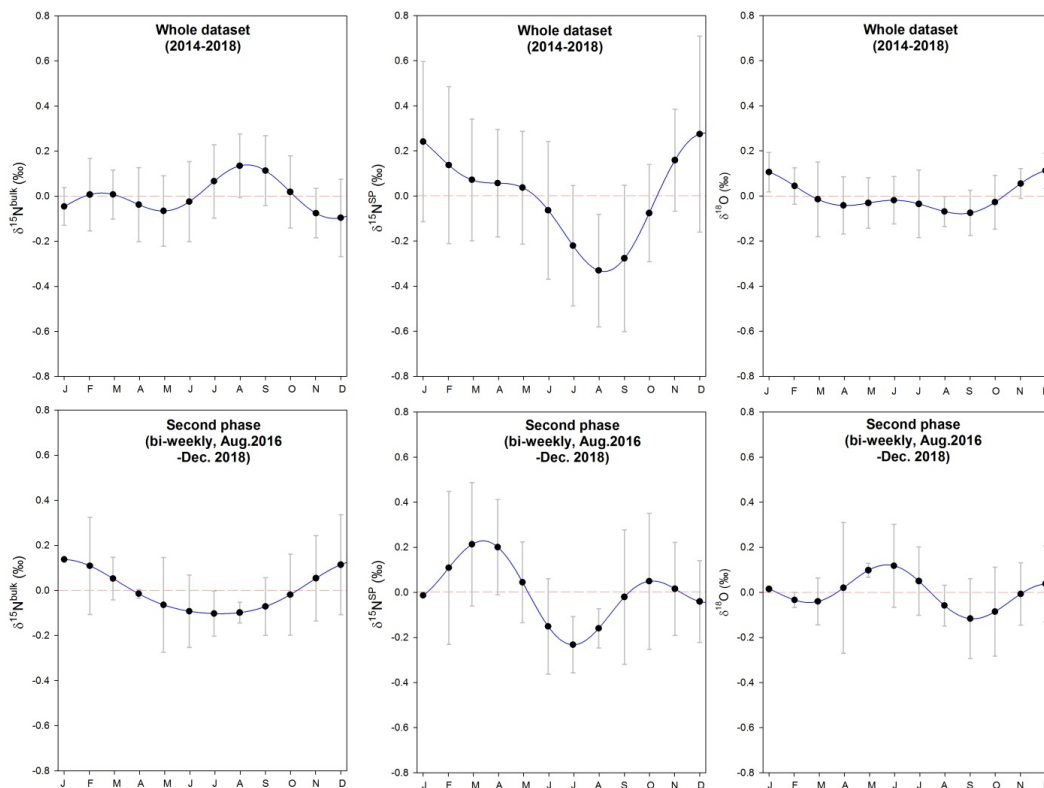


1000 **Figure 1a** *In situ* (10-min averages) and discrete measurements of N₂O mixing ratios from April 2014 to December 2018 at Jungfraujoch. *In situ* N₂O mixing ratio measurements were performed with GC-ECD method between April and December 2014. After that, OA-ICOS became the major analytical method for *in situ* measurements. Discrete sample points are presented as averages with error bars (one standard deviation). Annual N₂O growth rates determined by linear regression are given in the figure (uncertainty shown as one standard deviation). A sampling gap exists for discrete samples between February and August 2016.

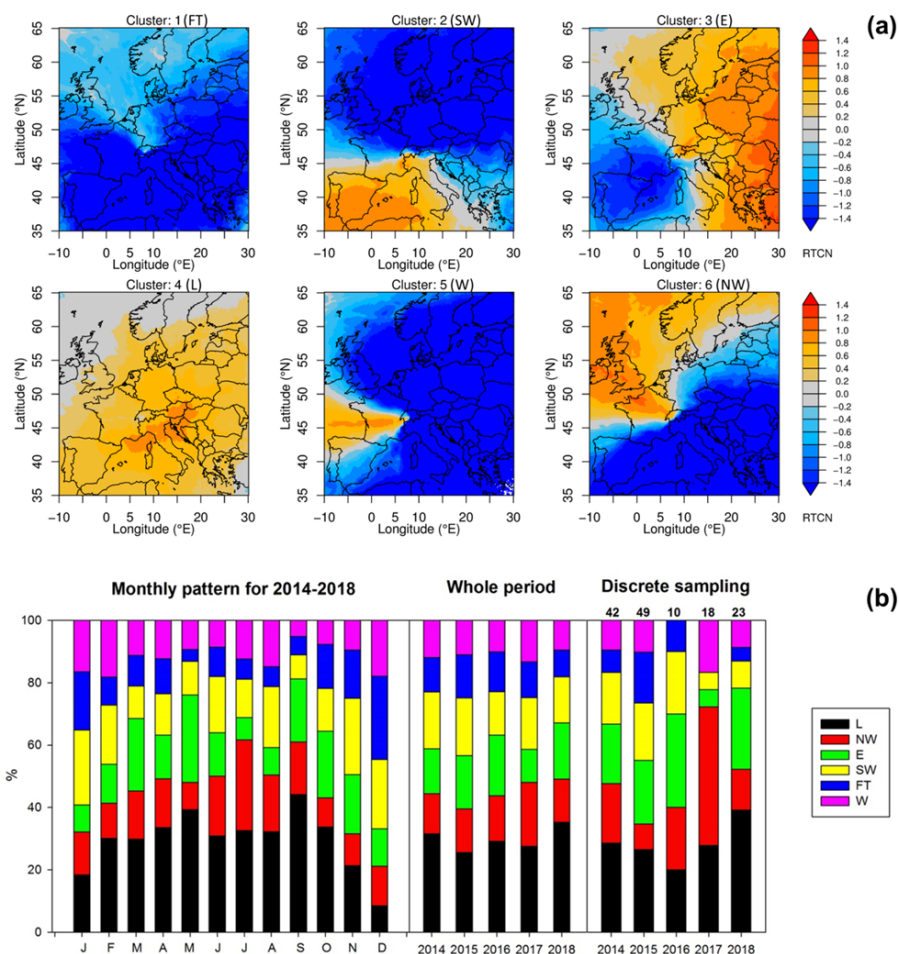
1005 **1b** Seasonality of N₂O mixing ratios at Jungfraujoch derived from *in situ* measurements. Datasets with/without GC-ECD measurements are compared for seasonality evaluation. The NLS model simulation for time-series gives the detrended seasonality, with error bars indicating one standard deviation of monthly residuals.



1010 **Figure 2** Time-series of isotopic composition of atmospheric N₂O observed at Jungfraujoch from April 2014 to December 2018. Error bars indicate one standard deviation of repeated measurements. Blue lines indicate the simulated trends by the NLS model.



1015 **Figure 3** Seasonality of isotopic signatures of atmospheric N₂O observed at Jungfrauoch. Top panels: seasonality obtained using the whole dataset from April 2014 to December 2018; lower panels: seasonality obtained using bi-weekly data collected between August 2016 and December 2018. Red dashed lines refer to zero variability. The NLS model simulation for time-series gives the detrended seasonality, with error bars indicating one standard deviation of monthly residuals.



1020 **Figure 4a** Clusters of air mass transport regimes for Jungfraujoch shown as normalized surface source
 sensitivities over our sampling period. Cluster abbreviations refer to Free Troposphere (FT), Southwest
 (SW), East (E), Local (L), West (W) and Northwest (NW). The normalization was done by calculating the
 difference between cluster average source sensitivity and whole period average source sensitivities,
 1025 divided by the period average. Orange colors indicate the main source regimes in each cluster, whereas
 blue colors indicate little to no influence on Jungfraujoch observations. The free tropospheric cluster
 showed lower than average surface sensitivity everywhere.

4b Cluster frequency of air mass transport regimes (%) shown as a monthly pattern (left) and interannual
 patterns for the whole periods (middle) and for the periods of discrete sampling (right). Numbers above
 the right figure indicate the total number of discrete samples per year.

1030

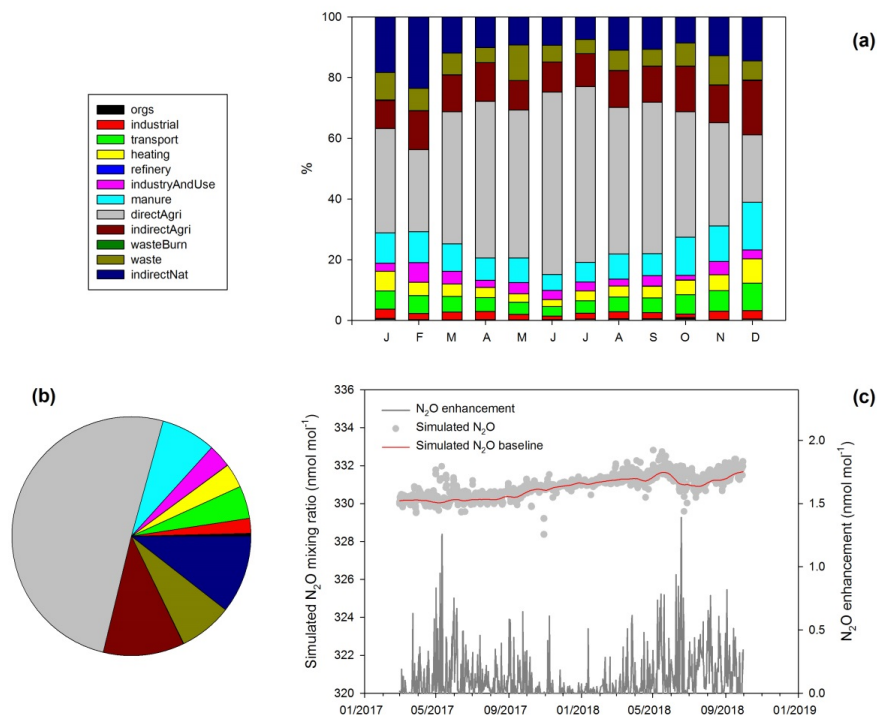
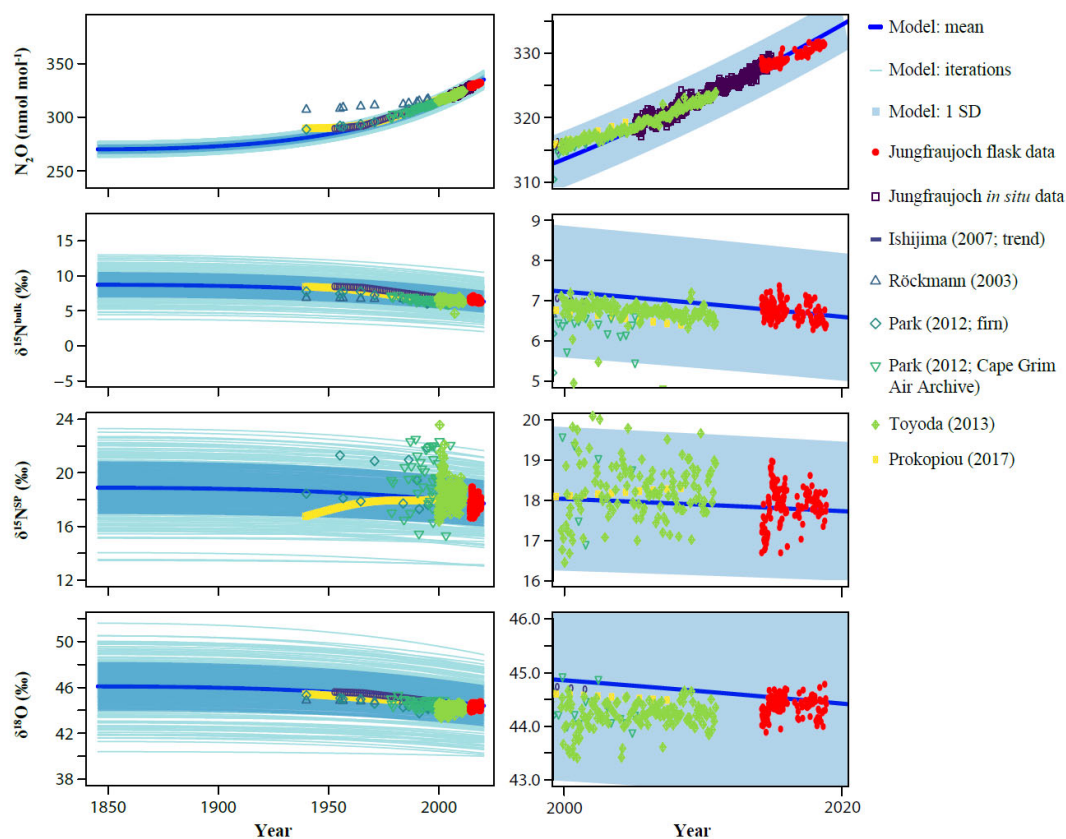


Figure 5a Mean monthly stacked-bar plots of source contributions (%) to atmospheric N₂O at Jungfraujoch derived from inversion modeling.

5b Overall contributions of N₂O sources responsible for emission to Jungfraujoch.

1035 **5c** Simulated 3-hourly N₂O mixing ratios, N₂O mixing ratio baseline and N₂O enhancements in nmol mol⁻¹.



1040 **Figure 6** Two-box model results showing the influence of anthropogenic emissions on N_2O mixing ratio
and isotopic composition in the troposphere. Left: full time range from the start of the anthropogenic
period (1845) to present day; Right: zoom to the last two decades. Isotopic measurements at Jungfraujoch
were used as the only constraint of current tropospheric N_2O isotopic composition for the model. See the
materials and method as well as the SI for more details and other input parameters. Atmospheric as well
as firn air measurements of $\delta^{15}\text{N}^{\text{bulk}}$, $\delta^{15}\text{N}^{\text{SP}}$ and $\delta^{18}\text{O}$ from the literature are presented for comparison.
1045 Blue shaded areas indicate one standard deviation of the model iterations.